AE International – North America

Atmospheric Environment 38 (2004) 3689–3711

ATMOSPHERIC ENVIRONMENT

www.elsevier.com/locate/atmosenv

Modeling particulate matter in the San Joaquin Valley with a source-oriented externally mixed three-dimensional photochemical grid model

Tony Held[a], Qi Ying[a], Ajith Kaduwela[b], Michael Kleeman[a,*]

[a] *Department of Civil and Environmental Engineering, University of California, One Shields Ave., Davis, CA 95616, USA*
[b] *The California Air Resources Board (CARB), 1001 I Street, Sacramento, CA 95812, USA*

Received 27 August 2003; accepted 25 February 2004

Abstract

Air pollution in California's San Joaquin Valley (SJV) rivals that of the Los Angeles area and ranks among the worst in the United States for particulate matter (PM) and ozone. The application and validation of an atmospheric chemical transport model to the SJV will aid in the design of emissions control programs to improve air quality. The extensive data required for meaningful Eulerian modeling of airborne PM in the SJV region were collected as a part of the 1995 Integrated Monitoring Study (IMS95). In the current study, the CIT-UCD source-oriented air quality model is applied to the IMS95 data set to verify model performance in the SJV. This article represents the first published application of a full-scale photochemical grid model with diagnostic meteorological data to simulate PM concentrations in the SJV and is the first study outside of the Los Angeles area to include complete PM model performance statistics.

The CIT-UCD model results show excellent agreement with most measurements collected during the IMS95 4–6 January 1996 modeling episode. The fractional bias (FBIAS) for SJV ozone and PM_{10} are approximately 0.16 and −0.19, respectively, for all SJV stations excluding Bakersfield. Most modeled criteria gases, PM precursor gases, and chemically speciated PM concentrations show strong agreement with their corresponding measurements at the Chowchilla, Fresno, Kern Wildlife Refuge, and Bakersfield sampling stations. Furthermore, the modeled PM size distribution of nitrate, ammonium ion, and sulfate agree well with cascade impactor measurements made at Bakersfield on 5 January 1996. Given the robust model agreement with both gas and condensed phase measurements, it appears that the CIT-UCD model adequately captures the fundamental transport and chemical reactivity of air pollutants in the IMS95 domain during a typical severe pollution episode. These results suggest that the CIT-UCD model can be used to explore control scenarios designed to improve air quality in the SJV.

Keywords: Air quality; Particulate matter; Source-oriented air quality model; San Joaquin Valley (SJV); California Regional PM_{10}/$PM_{2.5}$ Air Quality Study (CRPAQS); Integrated Monitoring Study (IMS95)

1. Introduction

The United States Environmental Protection Agency (EPA) has formulated National Ambient Air Quality Standards (NAAQS) for particulate matter (PM) with aerodynamic diameters less than 10 μm (PM_{10}) and 2.5 μm ($PM_{2.5}$). The PM standards are set such that sensitive members of the public will not experience negative health effects associated with the penetration of PM into the deep lung. PM_{10} NAAQS standards are violated in several California regions and the more stringent state PM standards are violated in most areas of the state indicating that air pollution in California represents a serious health problem (Alexis et al., 2002).

*Corresponding author. Tel.: +1-530-752-8386; fax: +1-530-752-7872.
E-mail address: mjkleeman@ucdavis.edu (M. Kleeman).

1352-2310/$ - see front matter © 2004 Elsevier Ltd. All rights reserved.
doi:10.1016/j.atmosenv.2004.02.053

California air quality sampling and modeling efforts have historically focused on the Los Angeles (LA) Metropolitan Area (South Coast Air Basin), but recent measurements have shown that air pollution in California's San Joaquin Valley (SJV) rivals LA in both the frequency and severity of air quality violations. For example, in 2002 the number of days exceeding the 8-h ozone standard in the SJV and LA air basins were 101 and 100, respectively, and in 2000 the PM_{10} maximum annual geometric mean in the SJV and LA air basins were 45.4 and 54.6 $\mu g\,m^{-3}$, respectively (Alexis et al., 2002). Based on preliminary data collected by the Californian Air Resources Board (CARB) in 1999 and 2000, peak 24-h averaged $PM_{2.5}$ concentrations in the SJV and LA air basins were 160 and 121 $\mu g\,m^{-3}$, respectively.

The EPA requires states to submit a State Implementation Plan (SIP) to demonstrate that either PM NAAQS are satisfied or that control strategies that will result in NAAQS compliance are being implemented. Given that the SJV routinely violates PM NAAQS, control strategies must be formulated to protect human health and welfare in this region. The determination of the best control strategy for PM is not always straightforward since PM results from both primary particle-phase emissions and from the non-linear reaction of precursor gas-phase species leading to the formation of secondary particulate matter. The design of a PM control strategy is further complicated by the fact that reductions in PM precursor emissions may conflict with SIP strategies enacted for ozone control.

Photochemical air quality models are useful tools that can predict the non-linear response of pollutant concentrations to changes in precursor emission rates. Confidence is established in the ability of an air quality model to predict the effect of emissions controls on pollutant concentrations by demonstrating that the model is able to predict existing pollutant trends during a representative air quality episode. Although statistical analyses for gas phase pollutants have previously been conducted in the SJV (Dabdub et al., 1999; Jacobson, 2001), to date, the only published studies including thorough PM performance statistics have focused on the Southern California Air Quality Study (SCAQS) conducted in Los Angeles in 1987 (Jacobson, 1997; Meng et al., 1998; Pai et al., 2000). Performance statistics must be calculated for other regions to establish confidence in PM model predictions outside the LA area.

The purpose of this article is to describe the ability of the CIT-UCD source-oriented photochemical air quality model to simulate both ozone and PM in the SJV during a typical pollution episode by calculating rigorous performance statistics. This study is based on the 1995 Integrated Monitoring Study (IMS95) data set collected in the winter of 1995–96 and represents the first published 3D grid modeling of PM in the SJV. The CIT-UCD source-oriented air quality model represents multiphase atmospheric chemistry at its fundamental level and provides deeper insight into the formation, transport, and fate of PM than can be inferred by more simplistic rollback or box modeling approaches. The focus of this paper is limited to model validation; future articles will explore source apportionment of both primary and secondary PM and detail the efficacy of various SJV PM control strategies.

2. The SJV and IMS95 study

The SJV includes Fresno, Kings, Madera, Merced, San Joaquin, Stanislaus, Tulare, and Kern counties covering approximately 25,000 square miles with approximately 10% of California's population (over 3 million people) (Alexis et al., 2002). The northern two-thirds of the SJV are primarily associated with agricultural activity, whereas the southern third is dominated by oil production (Solomon and Magliano, 1999a). Most urban areas are located near the major highways US-99 and I-5 that bisect the SJV. The two largest metropolitan areas in the SJV are Fresno (approximate population (AP) of 900,000) located in the north and Bakersfield (AP of 650,000) located in the south (Source: 1999 US Census). Together, these two cities constitute over 50% of the population in the SJV with the remaining people distributed in approximately 100 much smaller cities and rural areas.

PM measurements in the SJV show strong seasonal trends and demonstrate significant heterogeneity in particle composition. The most severe particulate air pollution episodes in the SJV typically occur during the winter months November–February. Wintertime PM_{10} is dominated by ammonium nitrate (50%), mobile sources (20%), and vegetative burning (15%) with approximately 70–80% of the PM_{10} mass contained in particles smaller than 2.5 μm in diameter (Magliano et al., 1999).

The IMS95 study was a subcomponent of the California Regional $PM_{10}/PM_{2.5}$ Air Quality Study (CRPAQS) that was designed, in part, to provide the meteorological, air quality, and emission inventory data required to simulate the SJV with Eulerian air quality models so that the effectiveness of potential PM control strategies could be evaluated. The IMS95 sampling effort included PM and gas phase measurements collected in the fall of 1995 and the winter of 1995–96. The primary purpose of the fall study was to determine the spatial representativeness of measurements and to identify scales of pollutant transport in the SJV based on 14 days of continuous saturation sampling. One of the goals of the winter sampling period was to collect data suitable for grid-based air quality modeling. Although

there have been previous air quality studies in the SJV, including the 1988 to 1989 Valley Air Quality Study (VAQS) (Chow et al., 1993), the extensive data requirements for meaningful PM Eulerian modeling of the region had not been collected until the IMS95 winter study.

Fig. 1 depicts the location of select IMS95 sampling sites, major roadways, and the topography of the SJV.

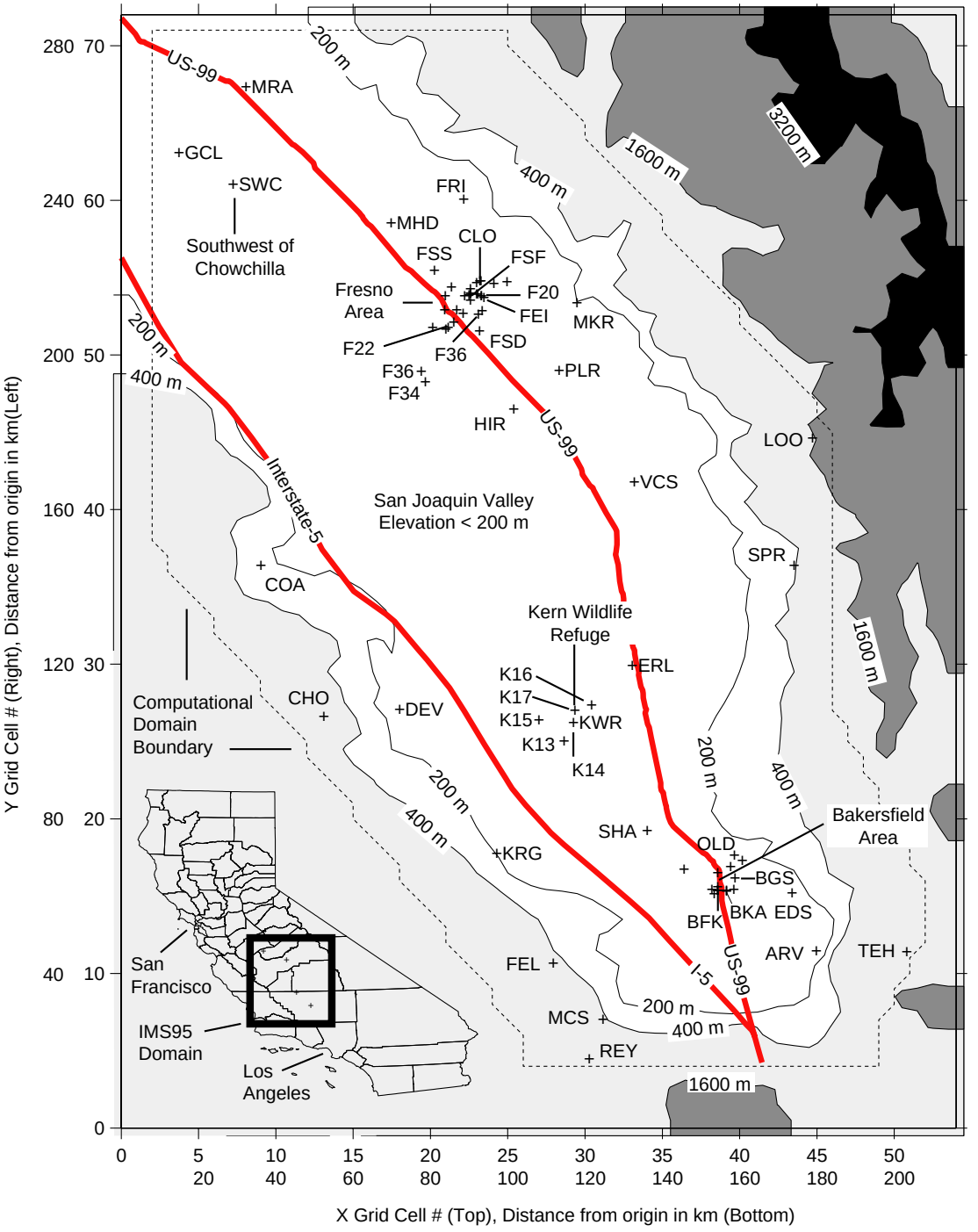

Fig. 1. IMS95 site map depicting select sampling sites, major roadways, and the topography of the SJV. The dashed inner line represents the computation boundary used in the current study.

Table 1
Site code, description, and coordinates for select IMS95 stations. Core stations are in bold. Lambert coordinates are based on latitude of projection, central meridian, 1st parallel, and 2nd parallel of 37°, 120.5°, 30°, and 60°, respectively. Grid cell refers to the IMS95 computational coordinate system

Code	SITE description	Coordinate				Elevation (m)
		Labert (km)		Grid cell		
		X	*Y*	*X*	*Y*	
MRA	Merced	5.8	30.6	7.7	67.4	55
GCL	Grover	−11.5	13.5	3.4	63.1	4
SWC	Southwest of Chowchilla	2.5	5.3	6.9	61.1	49
FSS	Fresno, northwest	54.5	−17.0	19.9	55.5	98
CLO	Clovis	68.5	−18.6	23.4	55.1	350
F20	Fresno, Central	63.9	−21.8	22.2	54.3	91
F25	Fresno, Central	65.4	−20.2	22.6	54.7	91
FEI	Fresno, Core Station	63.9	−23.0	22.2	54.0	91
FSF	Fresno, Central	63.5	−23.4	22.2	53.9	96
MKR	Mouth of Kings River	91.3	−24.6	29.1	53.6	145
F22	Fresno, southwest	59.6	−30.4	21.2	52.1	69
F28	Fresno, southwest	62.0	−28.2	21.8	52.7	80
F39	Fresno, southwest	60.3	−27.1	21.3	52.9	80
F31	Fresno, South	65.9	−28.3	22.7	52.6	91
F32	Fresno, South	66.8	−27.4	23.0	52.9	91
FSD	Fresno, South	66.2	−32.7	22.8	51.6	162
PLR	Parlier	86.8	−42.8	28.0	49.0	166
F34	Fresno, south by southwest	52.2	−45.8	19.3	48.3	60
F36	Fresno, south by southwest	51.1	−43.1	19.1	49.0	60
HIR	Hanford	75.1	−52.9	25.0	46.5	73
VCS	Visalia	106.3	−71.6	32.8	41.8	92
SPR	Springville	147.6	−93.3	43.2	36.4	304
ERL	Earlimart	105.7	−119.1	32.7	29.9	75
CHO	Cholame	25.9	−132.3	12.8	26.7	640
KWR	Kern wildlife refuge	90.5	−133.8	28.9	26.3	66
KRG	Kern ridge	70.6	−167.8	23.9	17.8	177
OLD	Oildale	132.1	−168.3	39.3	17.7	180
BGS	Bakersfield, Northwest	132.3	−174.1	39.4	16.2	151
BKA	Bakersfield, Central	130.1	−177.3	38.8	15.4	117
BFK	Bakersfield, Core Station	127.8	−177.4	38.2	15.4	116
EDS	Edison	147.0	−178.1	43.0	15.2	128
ARV	Arvin	153.3	−193.0	44.6	11.5	136
TEH	Tehachapi	176.7	−193.2	50.5	11.4	949
FEL	Fellows	85.4	−195.3	27.6	10.9	370
MCS	Maricopa	98.2	−210.7	30.8	7.1	289
REY	Reyes Station	94.6	−221.0	29.9	4.5	914

Key features of the SJV and the IMS95 sampling network will be outlined here; a more complete description of the IMS95 field program and its findings is provided by Magliano and Solomon (Solomon and Magliano, 1999a, b). The northwest corner of the SJV has no real physical boundary; rather, it is an arbitrary delineation point between the SJV and the Sacramento Valley (SV) that together constitute California's Central Valley. The SJV is bounded by the Sierra Nevada mountain range (peak elevation (PE) of 4300 m) on the east, the coastal mountain range (PE of 1530 m) on the west and the Tehachapi Mountains (PE of 1256 m) to the south (Chow et al., 1992). The majority of IMS95 air quality sampling was conducted on the valley floor since most of the SJV human population resides at elevations of 200 m or less. Sampling site coordinates for select IMS95 stations are presented in Table 1.

The IMS95 study included four core areas where intensive wintertime sampling was conducted. The core station identification codes were SWC (Southwest of Chowchilla), FEI (Fresno), KWR (Kern Wildlife Refuge), and BFK (Bakersfield). Chemically speciated PM_{10} and $PM_{2.5}$ measurements with 3 h sampling durations were made at the core stations. The SWC

station was designed to act as a boundary site to identify the influx of pollutants from the SV to the SJV. The KWR station represents a remote SJV locale with no significant nearby emissions of PM or its precursors. The FEI and BFK stations represent the major SJV urban areas of Fresno and Bakersfield, respectively. Model performance at the core stations will be highlighted in this study given the breadth and quality of PM data available in these areas. In addition to the core station measurements, standard gas phase air quality measurements and 24-h averaged PM_{10} and $PM_{2.5}$ mass measurements were made at over 90 stations distributed across the IMS95 domain.

3. Model formulation

The s*ource-oriented external mixture* CIT-UCD air quality model is based on the California Institute of Technology (CIT) family of atmospheric chemistry models. A detailed description of the CIT-UCD model and the history of its evolution have been presented previously (Eldering and Cass, 1996; Kleeman and Cass, 2001; Kleeman et al., 1997; McRae et al., 1982a) so only a brief overview of key model components and concepts are discussed here. *Externally mixed* refers to the model's ability to simulate an aerosol in which different particles of the same size can have different chemical compositions. *Source-oriented* indicates that PM emissions from different source categories are separately tracked by the model rather than combined into a single homogenized size distribution. This approach leads to a physically realistic aerosol simulation and allows for the deterministic source apportionment of PM.

In this study, the Finite Element Method (FEM) described by McRae et al. (1982b) was used for advection, semivolatile inorganic species thermodynamics and kinetics were based on the Aerosol Inorganic Module (AIM) developed by Wexler and Seinfeld (1991) as updated by Kleeman et al. (1997), secondary organic aerosol formation was based on the work of Pandis et al. (1992), the partitioning of semivolatile organic species into the particle phase was based on partitioning coefficients developed by Odum et al. (1996), dry deposition was based on the surface resistance boundary layer theory described by Russell et al. (1993), and gas phase chemical reactions were modeled using the SAPRC90 chemical mechanism developed by Carter (1990). Coagulation processes are not considered in this study because it has been shown that coagulation does not play an important role in shaping the particle mass distribution over a time scale of three days (Kleeman and Cass, 2001).

The CIT-UCD model was used to simulate the IMS95 aerosol with 15 discrete particle sizes ranging logarithmically in initial diameter from 10 nm to 10 μm. Each particle within the discrete size distribution was characterized by its diameter, number concentration, and chemical composition. Particles from individual emissions sources were grouped into nine source types: (1) crustal material other than paved road dust, (2) paved road dust, (3) wood smoke, (4) diesel engine exhaust, (5) non-catalyst equipped gasoline engine exhaust, (6) catalyst-equipped gasoline engine exhaust, (7) food cooking, (8) high sulfur-content fuel combustion, and (9) other particle sources. Two additional particle classes were used for sulfate and non-sulfate containing initial conditions yielding a simulation with a total of 11 distinct particle classes. Particles from each source type were separately tracked by a mathematical simulation of atmospheric advection, diffusion, deposition, and chemical reaction. Particles were not artificially mixed into a single atmospheric particle size and composition distribution (internal mixture), but rather, they existed separately from one another and interacted only through exposure to a common gas phase atmosphere.

4. Model application

3D Eulerian air quality model calculations were performed for the IMS95 4–6 January 1996 sampling episode within the computational domain illustrated in Fig. 1. The IMS95 region was represented by a 54×72 horizontal grid of 4 km square cells with 5 vertical layers. The vertical layers were logarithmically spaced with thickness equal to 39, 116, 154, 363, and 429 m yielding a total column depth of 1100 m. The total modeling domain included 19,440 cells, of which, 12,120 were in the computational domain. 100 processors (900-MHZ AMD) operating in parallel were used to drive the dynamic source-oriented CIT-UCD model over the IMS95 domain in real time.

4.1. Meteorological conditions

Surface meteorological conditions within the study domain were measured by monitoring stations operated by CARB, the National Climatic Data Center (NCDC), and the California Irrigation Management System (CIMIS). Measured values of solar radiation (19 sites), relative humidity (70 sites), temperature (70 sites), wind speed (18 sites), wind direction (18 sites), and fog (10 airports) were used to specify surface meteorological conditions throughout the study region based on Goodin's interpolation procedure (Goodin et al., 1979). Reductions of the surface UV irradiants due to cloud cover were estimated using the empirical equation described by Matthijsen et al. (2000).

The surface fields were augmented with upper elevation measurements to create interpolated 3D fields for certain meteorological variables. Rawinsonde

measurements collected near Fresno and Bakersfield provide vertical profiles of temperature and humidity in the domain. Rawinsonde and radar profiler measurements collected at six sites were used to interpolate the upper layer wind speed and wind direction. Transport was generally stagnant with low wind-flows from the northwest to the southeast during the study period.

Based on the rawinsonde data, the Holtzworth method (Holtzworth, 1967) was used to generate interpolated mixing depth fields that were verified and improved upon by detailed inspection of the temperature profiles. Calculated mixing depths were all well below 1000 m during the 3 day simulation period, with a typical afternoon maximum mixing depth of approximately 700 m. Thus, the modeled column depth of 1100 m encompasses the entire turbulent boundary layer during the modeling period.

Land use and land cover data were extracted from 1:100,000 (250 m resolution) United States Geological Survey (USGS) maps. Surface roughness heights and surface resistances for gaseous pollutants for each computational cell were estimated based on the cell's land use and land cover types using the method described by Russell et al. (1993).

4.2. Initial and boundary conditions

Initial conditions (ICs) and boundary conditions (BCs) for gas and PM species were based on pollutant concentrations measured at over 90 air quality stations collecting data throughout the 3-day study period. Concentrations of routinely monitored gas phase pollutants (O_3, NO, NO_2, SO_2, CO) were interpolated based on hourly measurements at over 30 monitoring sites throughout the SJV domain. Initial concentrations of gas phase nitric acid (HNO_3) and ammonia were interpolated based on more than 30 measurements, with approximately one half of these measurements collected near the urban centers of Fresno and Bakersfield. Hourly averaged reactive hydrocarbon (RHC) concentrations and 3-h averaged speciated RHC measurements were available continuously from 4 to 6 January 1996 near Fresno and Bakersfield. Speciated RHC fractions collected at these two sites were used to disaggregate RHC ICs and emissions.

Three-hour averaged PM data was collected at the four core IMS95 stations, and 24-h averaged data was collected at over 75 sampling stations. Cascade impactor data was collected at the Bakersfield site on 5 January 1996 from 12:00 to 15:00 and 21:00 to 24:00 using a Micro Orifice Uniform Deposit Impactor (MOUDI). The afternoon measurements form a more complete data set (i.e. no missing data) and were less likely to be affected by fog than the evening measurements since relative humidity was generally lower in the daylight hours. The afternoon impactor data was used to transform the speciated PM_{10} IC fields into size resolved PM fields suitable for model initialization. The PM ICs were partitioned into sulfate and non-sulfate containing fields that were tracked separately through model calculations.

Air quality data were interpolated for the specification of gas and PM ICs and BCs (not for the comparison of model results to measured values) based on a modified weighted average procedure described by Goodin (Goodin et al., 1979) represented as

$$C_i = \frac{\sum_{k=1}^{n} C_k \times W_k(r, R_a) \times A_k(r, R, R_a)}{\sum_{k=1}^{n} W_k(r, R_a)}, \quad (1)$$

$$W = \begin{Bmatrix} 1/r^2 & r < R_a \\ 0 & r > R_a \end{Bmatrix}, \quad (2)$$

$$A = \begin{Bmatrix} 1 & r < R \\ \exp(-\alpha \times (r - R)) & r > R \end{Bmatrix}, \quad (3)$$

$$\alpha = -\ln(0.03)/(R_a - R), \quad (4)$$

where C_i is the interpolated concentration at the ith grid cell based on the weighted averaged of surrounding data, C_k is the concentration at the kth measuring station, W is the weighting function, A is the attenuation function, α is the attenuation coefficient, n is the number of measurements in the domain, r is the radial distance from the ith grid cell to the kth measuring station, R is the "radius of unattenuated influence", and R_a is the "radius of attenuation". The attenuation coefficient is defined such that A is equal to 3% at $r = R_a$.

If one sets $R = R_a$ and A is set to unity, this formulation becomes the familiar inverse squared power law (ISPL) which was used to interpolate the meteorological fields. The ISPL approach works well when there are multiple measurements within R, however, if there is only one measurement within R, the ISPL approach results in a uniform circular concentration field surrounding the single point. To avoid remote circular fields, the modified interpolation approach was used to 'relax' interpolated fields to regional background concentrations at distances between R and R_a. Based on Blanchards' analysis, wintertime primary PM emissions have a radius of influence of approximately 10–30 km, whereas secondary pollutants tend to have a smooth and more regional distribution (Blanchard et al., 1999). Commensurate with these observations, (R/R_a) scaling distances of (5/40) and (150/200) km were used in this study for the interpolation of non-sulfate and sulfate particle fields, respectively. This approach represents an urban island effect for primary PM species such as elemental carbon and a smooth background field for secondary species such as sulfate. Although primary sulfate emissions are non-zero, the contribution of direct sulfate emissions to the overall SJV sulfate budget was found to be negligible when compared to secondary

formation pathways which justifies the classification of sulfate as a secondary species.

4.3. Emissions

Inventories describing the emissions of total organic gases (TOG), oxides of nitrogen (NO_x), oxides of sulfur (SO_x), ammonia (NH_3) and total suspended particulate matter (TSP) were compiled by CARB for the IMS95 study. All major area, point, and mobile source emissions within the study region were included in the inventory with a spatial resolution of 4 km and a temporal resolution of 1 h. Individual emissions records included a source classification category (SCC) number that could be used to assign detailed chemical speciation profiles to TOG and TSP emissions. TOG and TSP profiles used in this study were based on previous emissions source tests (Cooper et al., 1989; Harley et al., 1992, 1993; Hildemann et al., 1991a, b; Houck et al., 1989; Kleeman et al., 1999, 2000; Schauer et al., 1999a, b, 2001, 2002a, b; Taback et al., 1979).

Models for the emission of airborne particulate matter from mobile sources are relatively new and often contain large sources of uncertainty. In the current study, the spatial and temporal distribution of TSP emissions for each mobile source category (diesel, non-catalyst-equipped gasoline, catalyst-equipped gasoline) was retained, but the emissions were scaled to match the product of vehicle miles traveled (VMT) and measured emissions factors (Schauer et al., 1999b, 2002a) appropriate for that category. This procedure increased the TSP emission rate from mobile sources (tailpipe + tire dust) in the study region from 5030 to 8460 kg day^{-1}.

A summary of the emissions inventory on 4 January 1996 is shown in Table 2. On-road vehicles made the single largest contribution to non-methane organic gases (NMOG) and oxides of nitrogen (NO_x) emissions. PM_{10} emissions were dominated by dust sources, while residential wood combustion contributes significantly to $PM_{2.5}$ emissions. Detailed source contributions to ammonia emissions are not available because the ammonia inventory used in this study was preliminary.

In the course of this study it was discovered that excess NO emissions may be present in the emissions inventory around the Bakersfield area. An extra model simulation was conducted with NO_x emissions in the Bakersfield area reduced by 25% to test this hypothesis. The results of the basecase and the reduced NO_x simulation are discussed in the following sections.

5. Model results

A comparison of CIT-UCD modeled and measured concentrations for key PM and gas species are summarized in this section. Statistical metrics are defined and applied to air quality (AQ) species. Time series analyses for regional PM_{10}, regional ozone, and various core site AQ species are presented, and measured versus modeled PM size distributions are evaluated.

5.1. Model evaluation metrics

A variety of statistical measures have been developed to quantitatively specify air quality model performance (Cox and Tikvart, 1990; Lee and Irwin, 1995; Seigneur et al., 2000; Ward, 1994). Unless the modeled values are in exact agreement with measurements, each metric will result in a different interpretation of model performance. For example, a model prediction may have a low fractional bias, but the prediction may still poorly represent the paired peak concentrations. Furthermore, some statistical measures such as the normalized mean-squared error (NMSE) can lead to counterintuitive results. For example, the NMSE contribution of an over-prediction is dissimilar to an under-prediction, and in some cases NMSE performance can decrease when one includes additional modeled data points that are in perfect agreement with measured data (Poli and Cirillo, 1993).

To fully evaluate the CIT-UCD airshed model against the IMS95 data set, a consortium of performance metrics were calculated to complement the more qualitative graphical time series analysis. Most of the metrics used in this study are based on Seigneur's air quality performance evaluation research (Seigneur et al., 2000) that was specifically formulated for PM performance analysis. Metrics considered in this study include: (1) accuracy of unpaired peak (AUP), (2) accuracy of paired peak (APP), (3) mean error (BIAS), (4) mean absolute error (MAE), (4) fractional bias (FBIAS), (5) fractional absolute bias (FABIAS, referred to as fractional gross error by Seigneur et al.), (6) measured and modeled (M/M) mean (MEAN), (7) M/M mean absolute deviation (MAD), (8) M/M standard deviation (STD), and (9) M/M peak concentration.

The MEAN, MAD, STD, and PEAK metrics are standard statistical measures that require no further description. The AUP and APP vary from -1 (when the predicted value approaches 0) to ∞ (when the observed value approaches 0). Note that the peak predicted concentration for the AUP calculation is based on the largest modeled concentration found at grid cells where monitoring data was available, which is slightly different than the Seigneur et al. AUP formulation (Seigneur et al., 2000). The BIAS and MAE are traditional air quality metrics, which indicate the sign and absolute magnitude of model errors, respectively. FBIAS is used for air quality purposes because it is symmetric with regard to over- and under-predictions, and is bounded between $+2.0$ (extreme under-prediction) and -2.0

Table 2
Summary of the emissions inventory for the IMS95 model domain on 4 January 1996 in metric tons per day

Category code	TOG	NMOG	NO_X	CO	SO_X	NH_3	TSP	PM_{10}	$PM_{2.5}$
Fuel combustion									
Agricultural	7.2	6.9	51.6	39.4	6.1	0	4.1	3.9	3.7
Oil and gas production	9.3	3.7	71.0	6.9	3.9	0	2.0	2.0	2.0
Petroleum refining	0.1	0.1	2.0	0.3	13.0	0	0.3	0.3	0.3
Other manufacturing/industrial	0.2	0.1	15.9	1.5	3.5	0	0.4	0.4	0.3
Electric utilities	0	0	0	0	0	0	0	0	0
Other service and commerce	8.7	3.5	36.2	2.1	1.1	0	1.3	1.3	1.3
Residential	28.4	12.7	9.2	163.6	0.5	1.0	25.2	22.5	21.8
Other	0.1	0.1	1.2	0.5	0.2	0	0.1	0.1	0.1
Total	54.0	27.1	187.1	214.2	28.2	1.0	33.4	30.5	29.5
Waste burning									
Agricultural debris	3.4	2.5	0.9	18.3	0	0	2.4	2.0	2.0
Range management	0.2	0.2	0	2.0	0	0	0.4	0.3	0.3
Forest management	0.3	0.2	0.0	2.0	0	0	0.4	0.4	0.3
Incineration	0	0	0	0	0	0	0	0	0
Other	8.5	3.3	0.5	35.3	0.1	0	4.8	4.7	4.4
Total	12.5	6.2	1.4	57.6	0.1	0	7.9	7.4	7.0
Solvent use									
Dry cleaning	0.6	0.6	0	0	0	0	0	0	0
Degreasing	10.5	10.5	0	0	0	0	0	0	0
Architectural coating	1.1	1.1	0	0	0	0	0	0	0
Other surface coating	8.2	8.0	0	0	0	0	0.0	0.0	0.0
Asphalt paving	1.1	1.1	0	0	0	0	0	0	0
Printing	0.8	0.8	0	0	0	0	0	0	0
Consumer products	0	0	0	0	0	0	0	0	0
Industrial solvent use	6.0	6.0	0	0	0	0	0	0	0
Other	0.5	0.4	0	0	0	0	0	0	0
Total	28.9	28.5	0	0	0	0	0.0	0.0	0.0
Petroleum process, storage & transfer									
Oil and gas extraction	42.4	27.8	0	0	0	0	0	0	0
Petroleum refining	0	0	0	0	0	0	0	0	0
Petroleum marketing	12.6	5.3	0	0	0	0	0	0	0
Other	0.0	0.0	0	0	0	0	0	0	0
Total	55.0	33.1	0	0	0	0	0	0	0
Industrial processes									
Chemical	0.7	0.5	0.0	0	0.2	0	1.3	1.2	1.2
Food and agricultural	6.2	5.6	7.3	1.7	0.5	0	6.4	5.1	3.9
Mineral processes	0.2	0.2	14.7	0.2	4.0	0	2.9	1.8	1.2
Metal processes	0	0	0.0	0	0	0	0.0	0.0	0.0
Wood and paper	0	0	0	0	0	0	0.1	0.0	0.0
Other	0.0	0.0	0	0.1	0	0	0.0	0.0	0.0
Total	7.0	6.3	22.0	2.0	4.7	0	10.8	8.1	6.2
Miscellaneous processes									
Pesticide application	0	0	0	0	0	0	0	0	0
Fertilizer application	0	0	0	0	0	34.6	0	0	0
Soils	0	0	0	0	0	16.1	0	0	0
Farming operations	312.3	93.7	0	0	0	0	61.4	28.1	5.4

Table 2 (*continued*)

Category code	TOG	NMOG	NO_X	CO	SO_X	NH_3	TSP	PM_{10}	$PM_{2.5}$
Construction and demolition	3.3	3.2	29.2	13.5	3.7	0	38.5	23.4	6.4
Entrained road dust-paved	0	0	0	0	0	0	83.6	35.6	6.6
Entrained road dust-unpaved	0	0	0	0	0	0	60.5	35.9	7.9
Unplanned fires	0.1	0.1	0.0	0.9	0	0	0.1	0.1	0.1
Fugitive windblown dust	0	0	0	0	0	0	6.3	3.7	0.8
Waste disposal	191.9	3.3	0	0	0	0	0	0	0
Natural sources	0	0	0	0	0	0	0	0	0
Other	0	0	0	0	0	0	0	0	0
Total	507.5	100.3	29.2	14.4	3.7	50.7	250.4	126.8	27.2
On-road vehicles									
Diesel vehicles	5.2	5.2	85.5	20.9	0.8	0	1.5	1.3	1.2
Catalyst gasoline vehicles	85.4	75.0	140.5	1,546.4	0.3	2.1	2.0	0.9	0.8
Non-cat gasoline vehicles	65.7	64.8	0	0	0.0	0	5.0	4.4	4.4
Other	8.9	8.9	0	0	0	0	0	0	0
Total	165.2	153.9	226.0	1,567.3	1.1	2.1	8.5	6.6	6.4
Other mobile									
Off-road vehicles	4.8	3.9	0.3	16.4	0	0	0.0	0.0	0.0
Trains	0.8	0.8	15.9	2.5	0.5	0	0.4	0.4	0.4
Aircraft-government	3.3	3.0	1.1	6.4	0.0	0	0.2	0.2	0.2
Aircraft-other	6.6	5.9	1.5	46.6	0.2	0	0.1	0.1	0.1
Mobile equipment	0.4	0.4	2.3	1.2	0.3	0	0.2	0.2	0.2
Total	16.0	14.0	21.0	73.1	0.9	0	0.9	0.9	0.8
Other sources	102.1	78.0	39.4	89.6	2.4	121.5	11.0	6.4	3.3
Total for all categories	948.2	447.3	526.1	2,018.2	41.1	175.3	322.8	186.7	80.4

(extreme over-prediction) (Cox and Tikvart, 1990). The FABIAS is the positive complement to the FBIAS metric and varies from 0 (perfect model agreement) to 2.0 (extreme over- or under-prediction).

5.2. Regional performance of key PM and gas phase species

Table 3 summarizes regional model performance metrics for total mass (MASS), nitrate (NO_3^-), ammonium ion (NH_4^+), organic compounds (OC), elemental carbon (EC), sulfate (SO_4^{2-}), sodium (Na^+), and chloride (Cl^-) for both $PM_{2.5}$ and PM_{10} size cuts. In addition, metrics are presented for key gaseous species including ozone (O_3), carbon monoxide (CO), ammonia (NH_3), nitric oxide (NO), nitrogen dioxide (NO_2), reactive hydrocarbons (RHC), and sulfur dioxide (SO_2). For regulatory purposes, a grid model's ability to predict PM_{10}, $PM_{2.5}$, and ozone are paramount, so model performance for these three species will be analyzed in the greatest detail.

The distinction between EC and OC is operationally defined and is known to be a strong function of measurement technique (Schauer et al., 2003). OC is often used to indicate the concentration of organic carbon (carbon atoms) or organic compounds (carbon and associated hydrocarbon elements). IMS95 EC and OC (organic carbon) concentrations were measured based on the thermal-optical reflectance method (Chow et al., 2001) whereas the emissions database is based on the NIOSH method (NIOSH, 1996). To ensure consistency, all IMS95 measurements were converted to the NIOSH system. The IMS95 EC and OC measurements were adjusted with the following formulae; $EC_a = 0.5 \times EC$, $OC_a = (OC + 0.5 \times EC) \times 1.4$, where EC_a is the adjusted elemental carbon, EC is the IMS95 elemental carbon, OC_a is adjusted organic compounds, and OC is the IMS95 organic carbon consistant with the analysis of Schauer et al. (2003). This approach effectively shifts half of the EC concentration to OC and converts organic carbon to organic compounds with the multiplier of 1.4 (Schauer and Cass, 2000). The ratio of organic compound mass to organic carbon mass is a

Table 3
Measured and CIT-UCD modeled statistics and performance metrics for the 4–6 January 1996 SJV episode

Species	Units or cut size	Region code	Num. of points	MEAN		MAD		STD		PEAK		AUP	APP	BIAS	MAE	FBIAS	FABIAS
				Meas.	Mod.	Meas.	Mod.	Meas.	Mod.	Meas.	Mod.						
MASS	$PM_{2.5}$	a	108	40.2	58.7	17.7	26.0	24.2	31.9	146.6	146.3	0.00	−0.20	18.5	20.8	−0.38	0.43
MASS	PM_{10}	a	216	54.2	71.5	20.5	28.3	26.4	34.4	162.4	178.7	0.10	−0.19	17.3	20.8	−0.26	0.33
MASS	$PM_{2.5}$	b	24	28.0	39.2	8.9	9.0	10.6	10.5	45.5	56.3	0.24	0.03	11.3	13.8	−0.36	0.43
MASS	PM_{10}	b	24	38.1	45.7	9.8	10.6	11.4	12.9	55.7	69.8	0.25	−0.11	7.5	13.5	−0.18	0.33
MASS	$PM_{2.5}$	c	24	55.0	73.4	25.4	21.1	32.6	26.3	146.6	117.6	−0.20	−0.20	18.4	20.8	−0.39	0.41
MASS	PM_{10}	c	81	61.7	78.3	23.9	19.4	29.7	23.5	162.4	131.8	−0.19	−0.19	16.6	19.0	−0.30	0.33
MASS	$PM_{2.5}$	d	24	30.3	39.1	10.4	8.9	12.4	12.1	53.7	64.5	0.20	−0.30	8.9	11.9	−0.28	0.34
MASS	PM_{10}	d	33	36.6	43.9	9.3	9.3	11.4	12.4	58.2	69.0	0.19	0.05	7.2	8.4	−0.19	0.21
MASS	$PM_{2.5}$	e	24	53.4	92.8	18.9	29.6	24.5	34.6	113.8	146.3	0.29	0.17	39.4	40.0	−0.54	0.55
MASS	PM_{10}	e	57	66.9	102.0	18.3	29.9	24.0	35.7	145.6	178.7	0.23	−0.05	35.1	37.4	−0.40	0.44
MASS	$PM_{2.5}$	f	12	28.7	39.3	7.4	12.8	10.0	17.2	46.6	79.7	0.71	−0.30	10.6	14.2	−0.29	0.39
MASS	PM_{10}	f	21	37.3	35.8	10.8	9.4	13.0	15.9	63.6	87.7	0.38	−0.46	−1.5	10.0	0.05	0.25
MASS	$PM_{2.5}$	g	84	36.5	49.0	16.2	18.2	22.9	23.3	146.6	117.6	−0.20	−0.20	12.5	15.3	−0.33	0.40
MASS	PM_{10}	g	159	49.7	60.6	19.9	22.3	25.8	26.5	162.4	131.8	−0.19	−0.19	10.9	14.8	−0.21	0.30
NO_3^-	$PM_{2.5}$	a	96	15.3	18.8	6.1	6.9	7.4	8.6	37.9	43.4	0.15	−0.30	3.5	6.1	−0.23	0.38
NO_3^-	PM_{10}	a	138	16.1	19.1	5.5	6.9	6.7	8.6	32.5	43.7	0.34	0.31	2.9	5.0	−0.17	0.30
NH_4^+	$PM_{2.5}$	a	96	4.7	7.3	1.8	2.1	2.2	2.6	10.5	14.7	0.40	−0.07	2.7	2.7	−0.47	0.48
NH_4^+	PM_{10}	a	144	5.8	7.4	1.8	2.1	2.2	2.6	10.8	14.7	0.36	0.36	1.6	1.9	−0.27	0.31
OC	$PM_{2.5}$	a	96	15.6	17.1	11.8	12.4	16.2	14.8	102.3	55.1	−0.46	−0.64	1.6	6.3	−0.12	0.34
OC	PM_{10}	a	147	18.3	19.0	11.9	12.1	15.0	14.2	68.2	57.7	−0.15	−0.51	0.6	6.6	−0.02	0.34
EC	$PM_{2.5}$	a	96	1.8	3.3	1.3	2.3	1.7	3.0	11.9	14.5	0.22	−0.46	1.5	1.7	−0.55	0.61
EC	PM_{10}	a	147	2.3	3.7	1.5	2.3	1.8	3.0	11.9	15.0	0.79	−0.34	1.3	1.5	−0.41	0.48
SO_4^{2-}	$PM_{2.5}$	a	96	2.3	3.2	0.7	0.9	0.9	1.1	4.2	6.5	0.54	−0.39	0.9	1.1	−0.37	0.45
SO_4^{2-}	PM_{10}	a	144	2.7	3.4	0.6	0.9	0.8	1.1	4.6	6.5	0.41	−0.44	0.6	0.9	−0.20	0.31
Na^+	$PM_{2.5}$	a	33	0.1	0.1	0.0	0.0	0.0	0.0	0.2	0.2	0.01	−0.49	0.0	0.1	−0.53	0.79
Na^+	PM_{10}	a	183	0.1	0.1	0.1	0.0	0.1	0.0	0.4	0.2	−0.49	−0.74	0.0	0.1	−0.01	0.67
CL^-	$PM_{2.5}$	a	105	0.1	1.6	0.2	0.4	0.2	0.5	1.0	3.1	2.16	0.72	1.4	1.4	−1.71	1.71
CL^-	PM_{10}	a	192	0.2	1.5	0.2	0.2	0.3	0.4	1.3	3.1	1.31	0.27	1.4	1.4	−1.64	1.64
O_3	ppb	a	1368/57	25.1	19.8	7.8	7.9	10.1	9.5	48.5	40.0	−0.18	−0.33	−5.3	7.1	0.28	0.36
O_3	ppb	g	1008/42	25.9	21.8	7.0	5.8	9.2	7.1	48.5	40.0	−0.18	−0.33	−4.1	6.4	0.16	0.26
CO	ppm	a	648	1.1	1.2	0.7	0.6	1.0	0.8	7.4	5.3	−0.29	−0.72	0.1	0.5	−0.22	0.47
NH_3	ppb	a	213	22.9	12.9	17.7	5.5	29.7	6.9	252.4	33.3	−0.87	−0.88	−10.1	15.6	0.21	0.73
NO	ppb	a	1152	30.8	74.1	32.5	83.4	45.4	136.5	315.0	1070.9	2.40	−0.75	43.3	57.4	−0.24	0.94
NO	ppb	g	792	26.8	35.0	27.7	35.2	39.8	46.0	315.0	276.5	−0.12	−0.75	8.2	26.2	0.00	0.88
NO_2	ppb	a	1080	21.2	23.1	8.1	11.9	10.2	15.8	77.0	114.2	0.48	−0.66	1.9	8.9	0.03	0.43
NO_2	ppb	g	720	21.3	19.6	7.8	8.7	9.9	10.5	77.0	48.4	−0.37	−0.66	−1.6	6.4	0.14	0.37
RHC	ppmc	a	144	0.6	0.4	0.3	0.3	0.4	0.3	1.8	1.1	−0.41	−0.89	−0.2	0.3	0.32	0.62
SO_2	ppb	a	432	1.9	3.5	1.3	3.1	1.7	3.9	9.0	20.0	1.22	−0.33	1.6	2.0	−0.48	0.69

Region codes: (a) All data in the computational domain; (b) Chowchilla (SWC) area only; (c) Fresno (FEI) area only; (d) Kern Wildlife Refuge (KWR) area only; (e) Bakersfield (BFK) area only; (f) Areas not associated with core stations; (g) Data exluding the Bakersfield area.
Statistical abbreviations: MAD—mean absolute devition; STD—standard deviation; AUP—accuracy of unpaired peak; APP—accuracy of paired peak; BIAS—mean error; MAE—mean absolute error; FBIAS—fractional bias; FABIAS—fractional absolute bias.

function of the specific organic compounds involved. More highly oxidized organics tend to have higher ratios of organic compounds to organic carbon. A range of ratios have been suggested in the literature from 1.4 to 2.1 based on measurements made at different times and locations (Schauer et al., 2003). In the current winter study oxidant levels are relatively low and the conservative estimate of 1.4 seems appropriate. If a larger ratio was used, measured organic compound values would effectively increase.

Since sampling times were not the same for all PM species, the measured and modeled data were averaged such that only one sampling point was considered for each averaging time. For example, OC $PM_{2.5}$ was measured eight times a day (at 3 h resolution) at the four core sites for 3 days resulting in 96 ($8 \times 4 \times 3$) sampling points. Some PM species (i.e. PM_{10} MASS) were sampled at both 3- and 24-h resolutions. Since only one sampling point for each period was selected, a three-hour averaged site will contribute eight times as many

sampling points to domain-wide statistics as a 24-h averaged site. The ozone concentrations were filtered to compare measured versus modeled daily 8-h maximum concentrations because of their regulatory significance and statistical robustness. There were 19 ozone stations in the computational domain, which correspond to 1368 ($19 \times 3 \times 24$) hourly data points resulting in 57 (19×3) daily 8-h maximum ozone concentration points.

Domain-wide performance statistics are generally better for stations outside the area immediately surrounding Bakersfield. This is probably due to emission inventory issues, which result in excessive positive BIAS for PM and excess fresh-NO_x in the gas phase. The Bakersfield emission inventory is discussed in subsequent sections, but one should note that statistics including and excluding the Bakersfield area are listed in Table 3.

Air quality sampling stations are not evenly distributed across the SJV domain and tend to be more densely packed near the core sampling stations. Often times there are large emission and concentration gradients near urban areas in the SJV. Consider two grid cells (22,54) and (24,56) which approximately span the greater Fresno area. For the same time period, modeled PM_{10} EC at these two stations can differ by more than a factor of two or more (3.6 versus 8.3 $\mu g\,m^{-3}$) and modeled ozone can vary from 23 to 32 ppb. Regional performance figures presented in this article include all measurements from each urban area to fully resolve sharp spatial gradients.

6. PM_{10} and $PM_{2.5}$ model performance

The statistics summarized in Table 3 show that the mean (measured/modeled) $PM_{2.5}$, PM_{10}, and $PM_{2.5}$ to PM_{10} ratios are (40.2/58.7) $\mu g\,m^{-3}$, (54.2/71.5) $\mu g\,m^{-3}$, and (74/82)%. The region-wide measured $PM_{2.5}$ and PM_{10} are approximately 32% and 24% less than their modeled values, respectively, with excellent agreement in the fraction of PM_{10} that is in the $PM_{2.5}$ size range. The peak (measured/modeled) $PM_{2.5}$ and PM_{10} mass concentrations are (146.6/146.3) and (162.4/178.7) $\mu g\,m^{-3}$, respectively. $PM_{2.5}$ AUP, $PM_{2.5}$ APP, PM_{10} AUP, PM_{10} APP, are 0.00, −0.20, 0.10, and −0.19, respectively, indicating that modeled $PM_{2.5}$ and PM_{10} peaks are predicted within 20% of their measured values. The PM_{10} (with/without Bakersfield data) BIAS, MAE, FBIAS, and FABIAS, are (17.3/10.9), (20.8/14.8), (−0.26/−0.21), and (0.33/0.30), respectively, indicating that the model tends to slightly over-predict PM concentrations. When the Bakersfield data are excluded, most PM_{10} metrics show significant improvement, for instance, the BIAS and MAE and are reduced by 37% and 29%, respectively.

In order to fully understand the performance of PM mass predictions, a statistical analysis was also performed for the chemical constituents of airborne particulate matter. Sodium and chloride concentrations are extremely low (MEAN $<0.2\,\mu g\,m^{-3}$) in the SJV and are not significant contributors to $PM_{2.5}$ or PM_{10} mass. Regional sulfate and elemental carbon (EC) concentrations are also low (PM_{10} MEAN $<3\,\mu g\,m^{-3}$). Peak measured PM_{10} sulfate and EC are 4.6 and 11.9 $\mu g\,m^{-3}$, respectively. The PM_{10} MAE and BIAS for sulfate and EC are all less than 2 $\mu g\,m^{-3}$ indicating strong agreement for these species across the domain.

Nitrate, organic compounds, and to a lesser extent ammonium ion, are the principal components of the PM_{10} and $PM_{2.5}$ mass. The sum of these three species constitutes approximately 75% of mean PM_{10} and 90% of mean $PM_{2.5}$ mass. The PM_{10} BIAS (and FBIAS in parenthesis) for NO_3^-, OC, and NH_4^+ are 2.9 (−0.17), 0.6 (−0.02), and 1.6 (−0.27), respectively. The PM_{10} MAE (with measured STD in parenthesis) for NO_3^-, OC, and NH_4^+ are 5.0 (6.7), 6.6 (15.0), and 1.9 (2.2), respectively. These statistics demonstrate that modeled NO_3^-, OC, and NH_4^+ predictions are not significantly biased, and the absolute errors of these species are substantially lower than the standard deviations of the measured concentrations.

7. Gas phase model performance

Performance statistics for gas-phase species can be found in the lower half of Table 3. All ozone measurements in the computational domain during the study period are less than 55 ppb, which is well below the national 1-h ozone standard of 120 ppb. The peak 1-h ozone concentration (52 ppb) and the peak 8-h ozone concentration (48.5 ppb) were both measured at the FEL station on 6 January 1996. BIAS, FBIAS, mean 8-h daily maximum measured and modeled ozone concentrations are −5.3, 0.28, 25.1, and 19.8 ppb, respectively, which suggests that the model consistently underpredicts ozone. Most of this bias is due to the Bakersfield area stations of OLD, BGS, BKA, EDS, and ARV. Model performance for ozone outside the Bakersfield area is greatly improved, especially when considering the stations that are not adjacent to boundaries. BIAS, FBIAS, mean measured, and mean modeled values excluding the Bakersfield area are −4.1, 0.16, 25.9, and 21.8 ppb, respectively.

MEAN, STD, and PEAK NO_2 (measured/modeled) concentrations are (21.2/23.1), (10.2/15.8), and (77.0/114.2) ppb, respectively, with a MAE of 8.9 ppb, a BIAS of 1.9 ppb, and a FBIAS of 0.03. MEAN, STD, and PEAK NO concentrations are (30.8/74.1), (45.4/136.5), and (315.0/1070.9) ppb, respectively, with a MAE of

57.4 ppb, and a BIAS of 43.3 ppb. Excluding the Bakersfield area, MEAN, STD, and PEAK NO concentrations are (26.8/35.0), (39.8/46.0), and (315.0/276.5) ppb, respectively, with a MAE of 26.2 ppb, and a BIAS of 8.2 ppb. These values indicate that modeled NO_2 and NO outside the Bakersfield area show strong agreement with measured values, but NO is significantly over-predicted in the Bakersfield area leading to suppressed ozone predictions. Predicted ozone concentrations based on the emission inventory with NO_x emissions in the Bakersfield area reduced by 25% are presented as crossed lines in Fig. 3 for sites OLD, BGS, and BKA and clearly show that Bakersfield ozone model performance improves when local fresh NO_x emissions are reduced.

Carbon monoxide concentrations during the study period were quite low, averaging approximately 1.1 ppm with a peak measured concentration of 7.4 ppm. Carbon monoxide is not expected to be significant for regulatory purposes at these concentrations, but CO is a good indirect indicator of regional ventilation. The CO BIAS is approximately 0.1 ppm, suggesting that the specified mixing heights, wind fields, and advection routines used by the model are adequately parameterizing atmospheric dynamics near sampling stations. Modeled SO_2 concentrations show a tendency for over-prediction, but the MAE is only 2 ppb. Modeled RHC is relatively unbiased and is in good agreement with measured values with a BIAS, FBIAS, and MAE of −0.2 and 0.32, and 0.3 ppmc, respectively. The gaseous ammonia (measured/modeled) MEAN, STD, and PEAK concentrations are (22.9/12.9), (29.7/6.9), and (252.4/33.3), respectively, with an FBIAS of 0.21 and a BIAS of approximately −10.1 ppb. These results indicate that NH_3 concentrations are generally under-predicted and the domain-wide measured variably and peak concentrations are not captured in the model simulation. Presumably, measured and modeled NH_3 agreement would significantly improve with the formulation of a more complete NH_3 emission inventory. Since ammonium nitrate in the SJV appears to be HNO_3 limited, reasonable excesses or shortages of NH_3 in the emission inventory will not significantly affect the secondary production of PM.

Kumar et al. indicated that there were significant discrepancies between collocated HNO_3 measurements made by the Desert Research Institute (DRI) and the University of California Riverside's Center for Environmental Research and Technology (CERT) (Kumar et al., 1998). Kumar notes that "the DRI sequential filter sampler was not explicitly designed for, or tested, in high humidity environments" and that "samplers may not perform as expected when their components are coated with liquid water" (Kumar et al., 1998). No comparison is made to HNO_3 measurements in the current study.

7.1. Regional time series analysis

Measured and modeled PM_{10} time traces for major PM sampling stations in the SJV computational domain are presented in Fig. 2. All measurements within each computational grid cell are shown to illustrate the variability due to subgrid processes. The subplots are arranged based on the latitude of each station with SWC at the northern end of the domain and REY at the southern end. Modeled data are 3-h averaged at the core sites of SWC, FEI, KWR, and BFK, and are 24-h averaged elsewhere which corresponds to the measurement sampling intervals. The abscissa ranges from 0 to 150 $\mu g\,m^{-3}$ and obscures certain FEI and BFK data points; however, these clipped points are visible in Figs. 5 and 7.

Fig. 2 demonstrates that the CIT-UCD model shows excellent agreement with measured PM_{10} concentrations across the breath of the IMS95 domain throughout the sampling period. PM_{10} mass is well predicted at the core SWC site and shows excellent agreement with Fresno area measurements. Both predictions and measurements of PM_{10} mass concentrations at the foothill stations of SPR, DEV, and CHO are relatively low (typically $<50\,\mu g\,m^{-3}$) and are in solid agreement. Model performance at KWR and the nearby ERL station is quite good, reproducing both the magnitude and percentage buildup of PM_{10} during the sampling period. Bakersfield PM_{10} mass concentrations show reasonable agreement with measured values, but are over-estimated during certain evening periods due to emission inventory over-estimates which are discussed in a subsequent section. Model predictions at the southern TEH and REY stations agree with measurements, indicating that model performance at elevations greater than 900 m near the southern computational boundary is satisfactory.

Modeled and measured hourly ozone concentrations collected at all 19 IMS95 stations in the computational domain are presented in Fig. 3. Subplots are arranged based on the latitude of each station with MRA at the northern end of the domain and MCS at the southern end. Ozone measurements in the Chowchilla area (GCL and SWC) have missing data and are incomplete; the available data shows strong agreement with modeled concentrations. Similar to the PM performance, ozone concentrations are in excellent agreement with measured values in the greater Fresno area including the FSS, CLO, FSF, and FSD stations. Ozone tends to be over-predicted in the Kern Wildlife Refuge, but is typically within 10 ppb of the measured values which did not exceed 30 ppb. Model performance for ozone tends to degrade at sites near the domain boundary where there are steep changes in elevation. At the KRG (elevation 177 m), MCS (289 m), and FEL (370 m) stations, the measured ozone signal becomes significantly erratic

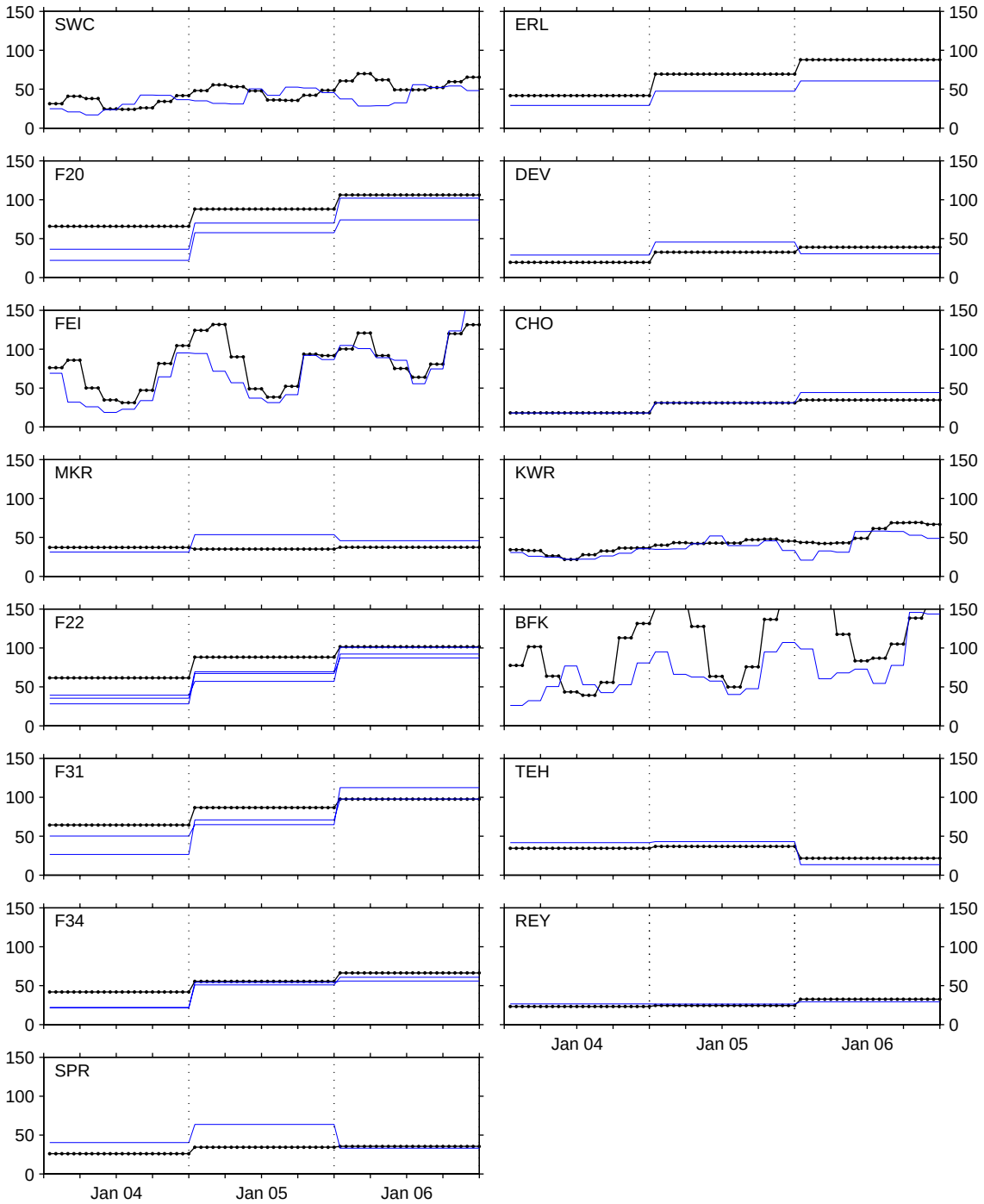

Fig. 2. Measured (solid lines) and predicted (dotted line) PM_{10} mass for the 4–6 January 1996 SJV episode. Modeled data is averaged to correspond to the minimum measurement averaging period available for each cell. All units are in $\mu g\,m^{-3}$.

compared to trends on the valley floor. The model is able to capture some of these trends, but the signals are not as closely matched as those observed on the valley floor near urban areas.

7.2. Time series analysis of core stations

Measured and modeled PM_{10} and gas phase concentrations near the SWC, FEI, KWR, and BFK core

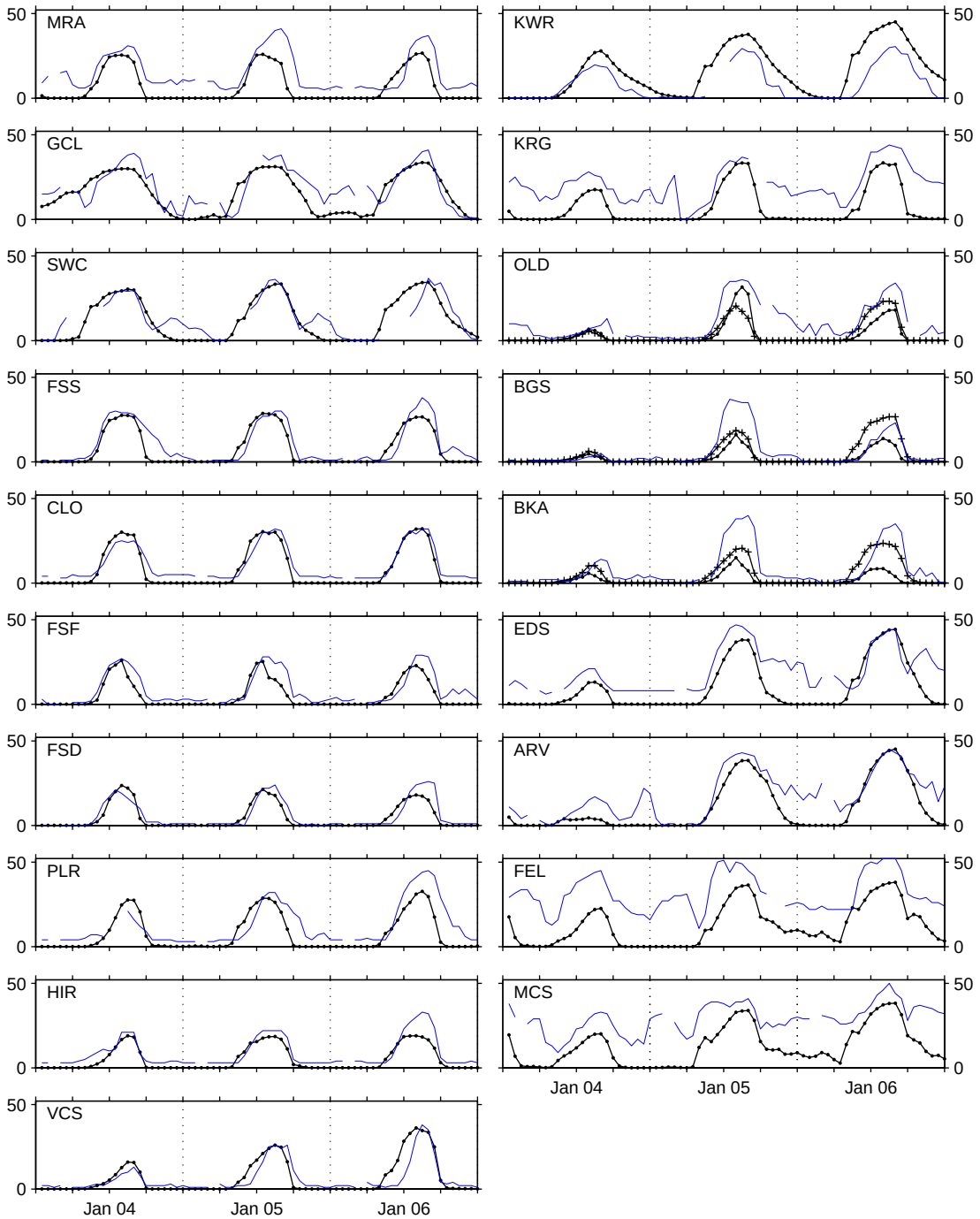

Fig. 3. Measured (solid line), predicted with basecase emissions database (dotted line), and predicted with reduced NO_x emissions (crossed line) ozone concentrations for the 4–6 January 1996 SJV episode. Concentrations are 1-h averaged and have units of ppb.

stations are presented in Figs. 4–7. Each figure contains measured and modeled PM_{10} MASS, NO_3^-, NH_4^+, OC, EC, SO_4^{2-}, and Na^+ in addition to gas phase concentrations of ozone, RHC, NH_3, NO, NO_2, SO_2, and CO. Missing measured data is represented by line breaks or the lack of a time series. $PM_{2.5}$ concentrations are not shown here but are qualitatively similar to PM_{10}.

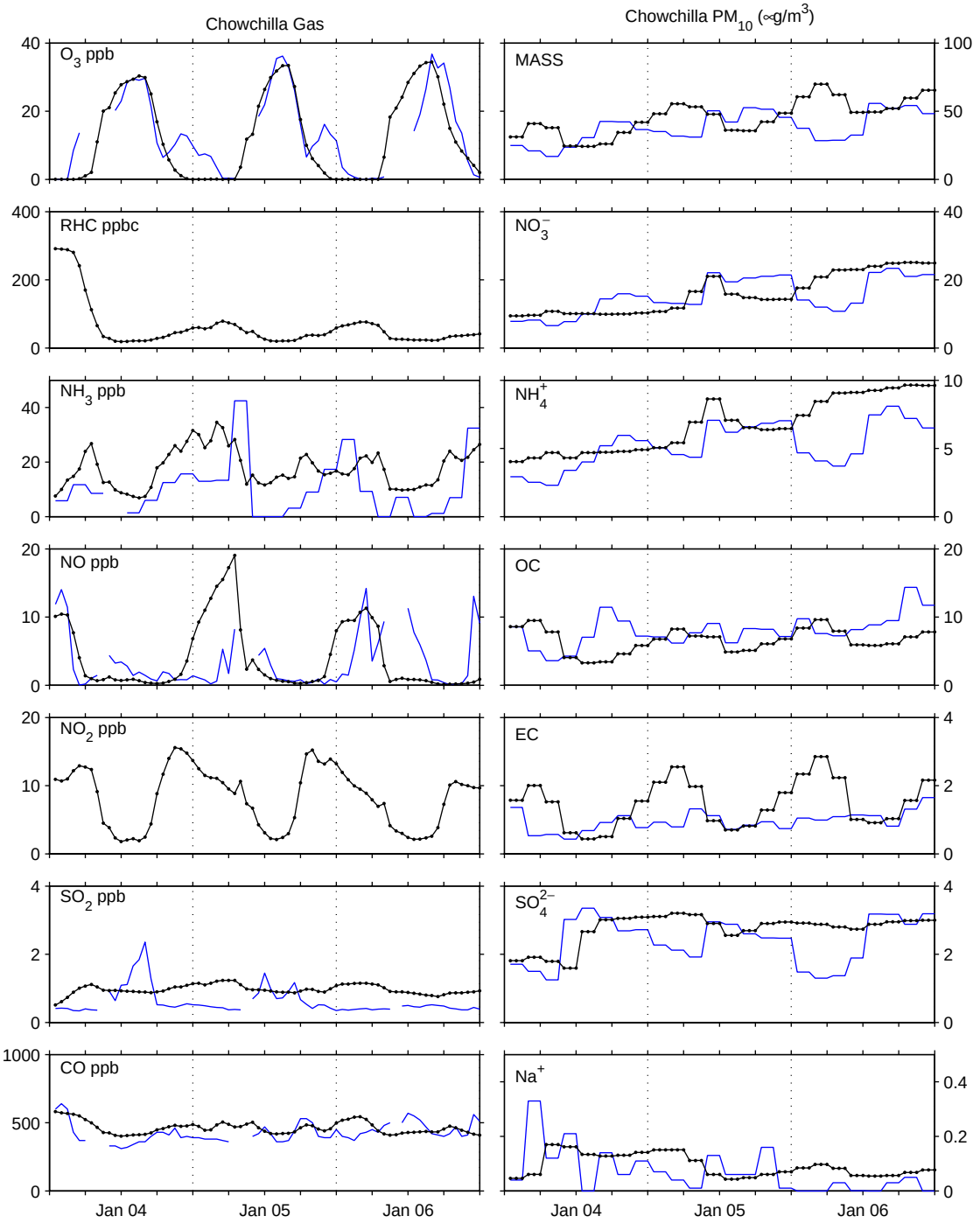

Fig. 4. Measured (solid lines) and modeled (dotted lines) time series for chemically speciated PM_{10} and key gas phase pollutants at the SWC (Chowchilla) core IMS95 station.

7.2.1. Chowchilla

Air quality predictions and measurements at Chowchilla are shown in Fig. 4. Particulate matter concentrations at SWC were relatively low compared to the rest of the domain and did not exceed $60\,\mu g\,m^{-3}$ during the study period. In general, 24-h averaged PM concentrations agree with model estimates at SWC, but certain diurnal features in the PM time-traces are not captured

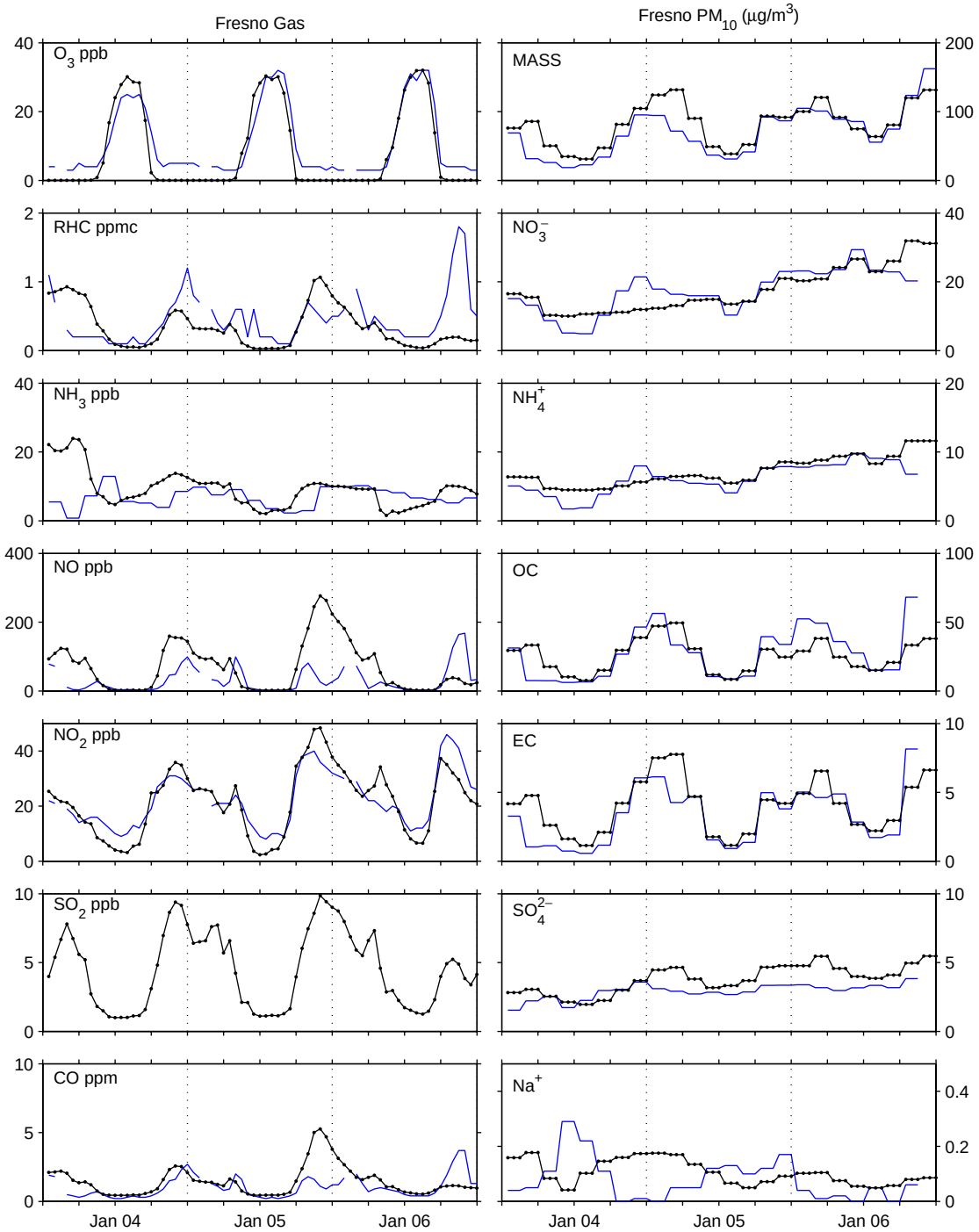

Fig. 5. Measured (solid lines) and modeled (dotted lines) time series for chemically speciated PM_{10} and key gas phase pollutants at the FEI (Fresno) core IMS95 station.

by the model. Interpretation of SWC performance is complicated by its proximity to the boundary and its potential domination by BC specification. Modeled PM_{10} mass and nitrate (the principal component of PM_{10} during the sampling event) show solid agreement with measurements. OC measurements are slightly under-predicted. Both measured and modeled Na^+ concentrations are negligible ($<0.5\,\mu g\,m^{-3}$). Modeled

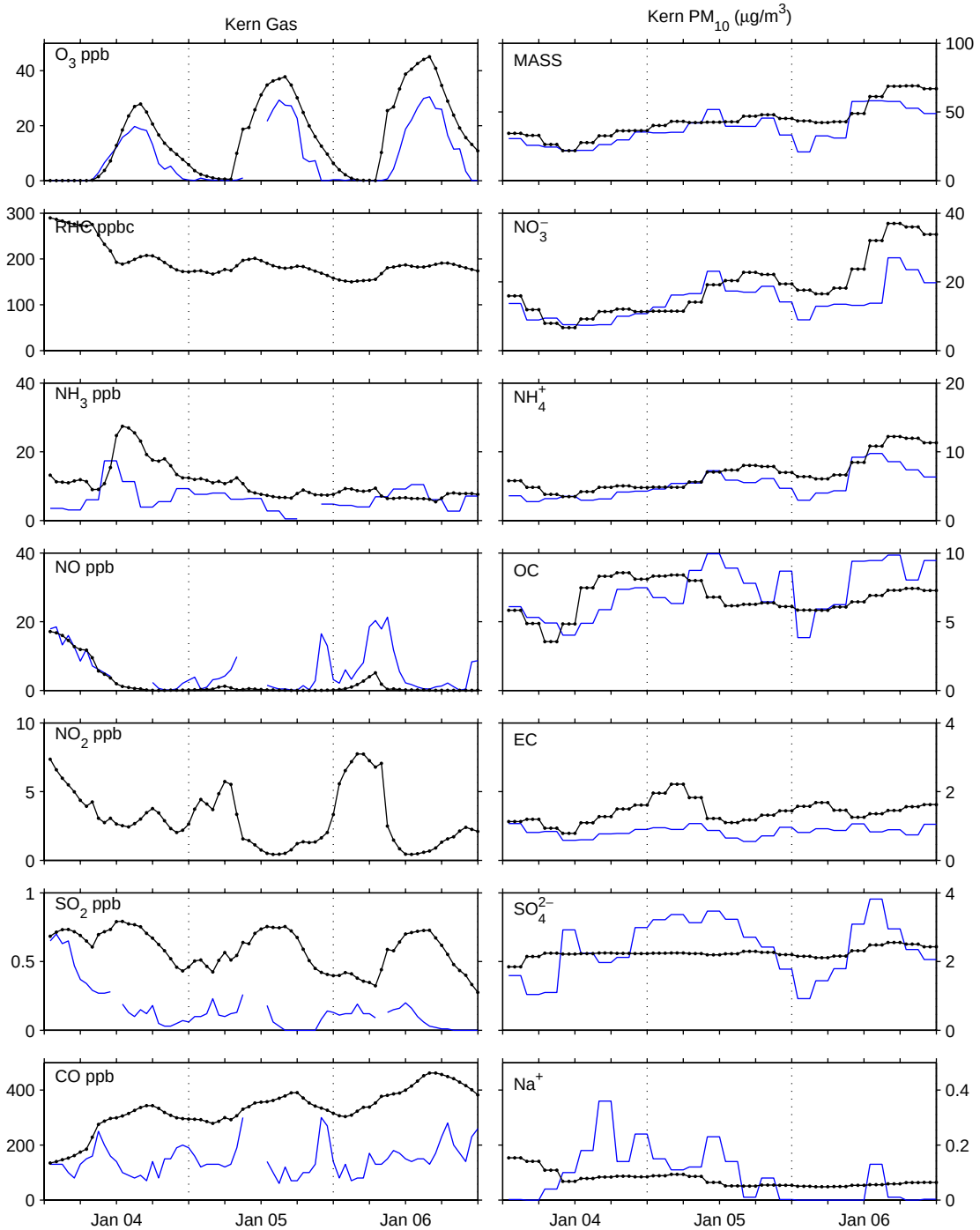

Fig. 6. Measured (solid lines) and modeled (dotted lines) time series for chemically speciated PM_{10} and key gas phase pollutants at the KWR (Kern Wildlife Refuge) core IMS95 station.

EC and SO_4^{2-} do not show the same diurnal pattern as their respective measurements but are typically within $1\,\mu g\,m^{-3}$ of the observations. Modeled ozone and CO show excellent agreement with measurements. The PM precursor species NH_3 and SO_2 show reasonable agreement with measurements. Overall, modeled

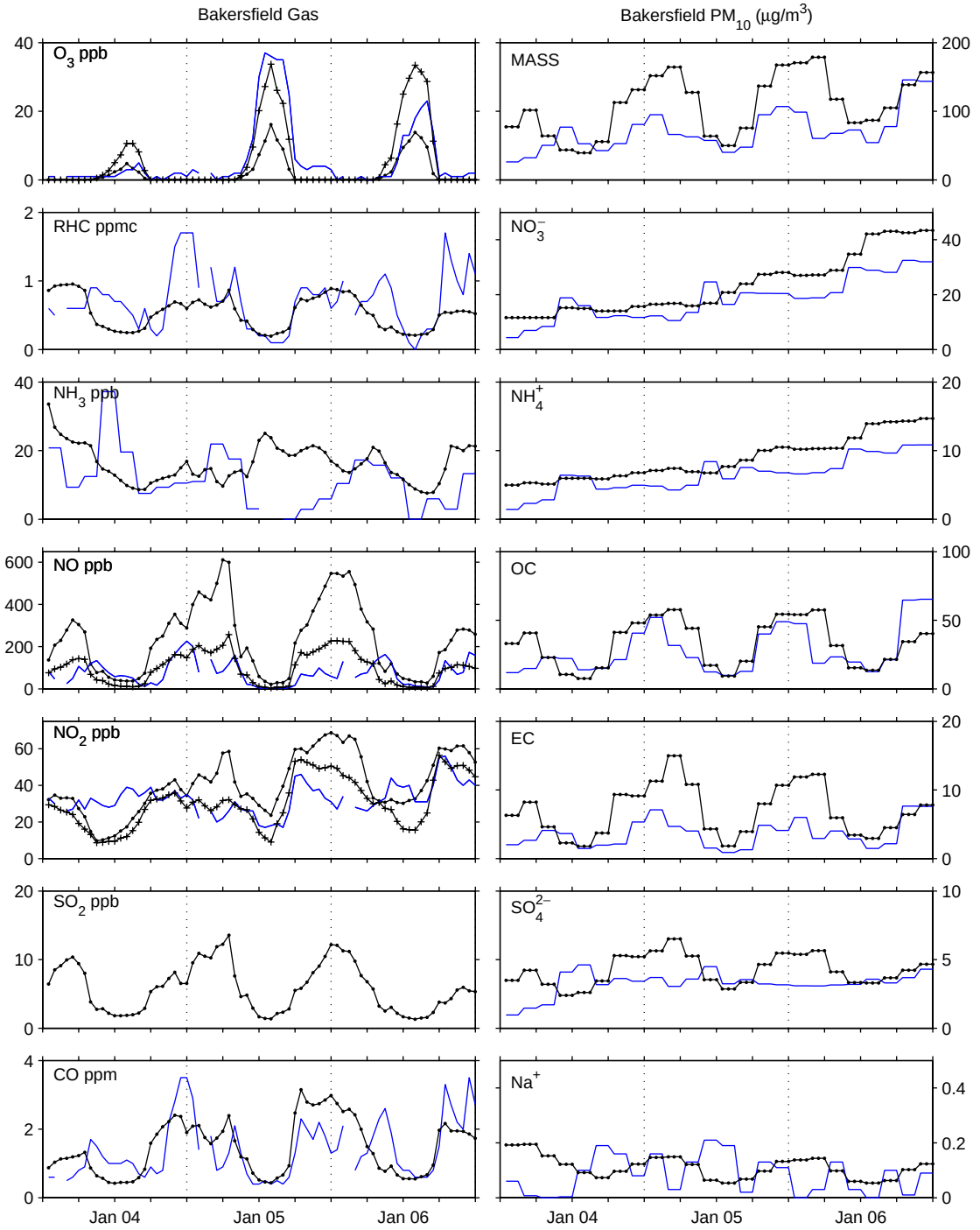

Fig. 7. Measured (solid line), predicted with basecase emissions database (dotted line), and predicted with reduced NO_x emissions (crossed line) model performance for chemically speciated PM_{10} and key gas phase pollutants at the BFK (Bakersfield) core IMS95 station.

predicted SWC concentrations show good agreement with measurements, which presumably results in correct mass flux specifications to the IMS95 domain interior.

7.2.2. Fresno

Air quality predictions and measurements at Fresno are shown in Fig. 5. Measured Fresno area $PM_{2.5}$

concentrations during this episode approached 150 μg m^{-3} and far exceed both state and national PM air quality standards. Overall model performance near Fresno is excellent for both gaseous and PM species. Modeled PM_{10} mass, OC, and EC show strong agreement with their corresponding measurement time traces. Daily production rates of NO_3^-, NH_4^+ and SO_4^{2-} species show solid agreement with measured values. Na^+ agreement is adequate given that both measured and modeled values are less than 0.3 μg m^{-3}. Ammonia is typically over-predicted, but, in general, shows reasonable agreement with measured values. Modeled concentrations of ozone and two key gaseous precursor species (NO_2 and RHC) are very similar to measured values. Finally, modeled CO shows good agreement with measured concentrations, which suggests that the ventilation rate and other key meteorological phenomena in the region are adequately parameterized.

7.2.3. Kern wildlife refuge

Air quality predictions and measurements at KWR are shown in Fig. 6. The KWR monitor was located in a remote area with virtually no nearby human population. Model performance at this site depends significantly on the proper specification of wind fields and pollutant transport. Given the additional complexity of modeling air quality at remote areas, overall KWR performance is adequate. Modeled ozone is typically within 10 ppb of measured values but is consistently over-predicted. RHC and NO_2 measurements were not collected so it is not feasible to determine the nature of the ozone bias at KWR.

As expected, PM_{10} concentrations at KWR were relatively low and did not exceed 58 μg m^{-3}. Modeled concentrations of PM_{10} mass, NO_3^- and NH_4^+ show good agreement with measured trends. Modeled OC is always within 5 μg m^{-3} of measured values; modeled EC is slightly over-predicted, but is typically within 1 μg m^{-3} of measured values. Modeled sulfate is typically within 1.5 μg m^{-3} of measured values and agrees well with 24-h averaged measurements.

7.2.4. Bakersfield

Air quality predictions and measurements at Bakersfield are shown in Fig. 7. Measured and modeled BFK CO show strong agreement indicating that the Bakersfield area mixing heights and ventilation rates are well parameterized. Modeled RHC also shows good agreement with the majority of measured concentrations except for a few measurements recorded in the evenings of 4 and 6 January. Modeled ozone concentrations near BFK are significantly under-predicted while NO is over-predicted when the basecase emissions inventory is used. Based on these trends, it is likely that NO_x emissions in the Bakersfield area are overestimated leading to suppressed ozone production. Fig. 7 includes ozone, NO, and NO_2 predictions that result when NO_x emissions in the region around Bakersfield are reduced by 25%. Modeled NO, NO_2, and ozone concentrations are in much closer agreement to observations under these conditions.

Modeled NO_3^- and NH_4^+ concentrations show good agreement with measured values throughout the study period except for the last 6 h when they are over predicted. Modeled OC, EC, and SO_4^{2-} show strong agreement with measured values. Although the predicted chemical components of PM_{10} show strong agreement with measurements, the modeled aggregate PM_{10} mass concentrations are significantly greater than measured values for isolated evening periods. The evening PM_{10} over-estimation is primarily caused by large (> 50% mass signal) 'other' PM species contributions from the 'crustal material other than paved road dust' emissions class. The basecase emissions database specifies uniform diurnal profiles for the crustal material source class. This emissions category is dominated by farming and construction activities that likely occur mainly during the daylight hours. The unrealistically large nighttime emissions of crustal material in the basecase inventory, coupled with strong nocturnal inversions, results in elevated PM_{10} mass predictions near the Bakersfield area during the evening of 4 January 1996. If a more realistic diurnal signal is applied to the crustal emissions, the modeled PM_{10} mass would likely show improved agreement with measured values.

7.3. Particle size distribution analysis

Dry aerosol predicted size distributions for NO_3^-, NH_4^+, SO_4^{2-}, EC, OC, and total carbon at Bakersfield between 12:00 and 15:00 on 5 January 1996 are shown in Fig. 8 along with their respective MOUDI measurements. When MOUDI size cuts are Stokes corrected assuming a PM density of 1.7 g cm^3, the sum of all mass collected on stages 2–10 should approximately equal PM_{10} mass. Comparison to collocated PM_{10} monitors indicates that MOUDI measurements typically under-predict filter-based sampling techniques. For comparison with predicted size distributions, the MOUDI data are normalized so that the summed mass from stages 2–10 agrees with collocated filter-based mass measurements. This approach assumes that the bias in the MOUDI measurements is not a strong function of particle diameter.

Model performance for ammonium ion and nitrate are excellent, exhibiting the same mode (0.3 μm), qualitative shape, and area under the curve as their associated MOUDI measurements. The qualitative shape of the modeled sulfate distribution is very similar to the MOUDI measurements; since the model tends to under-predict PM_{10} sulfate during this time period, the

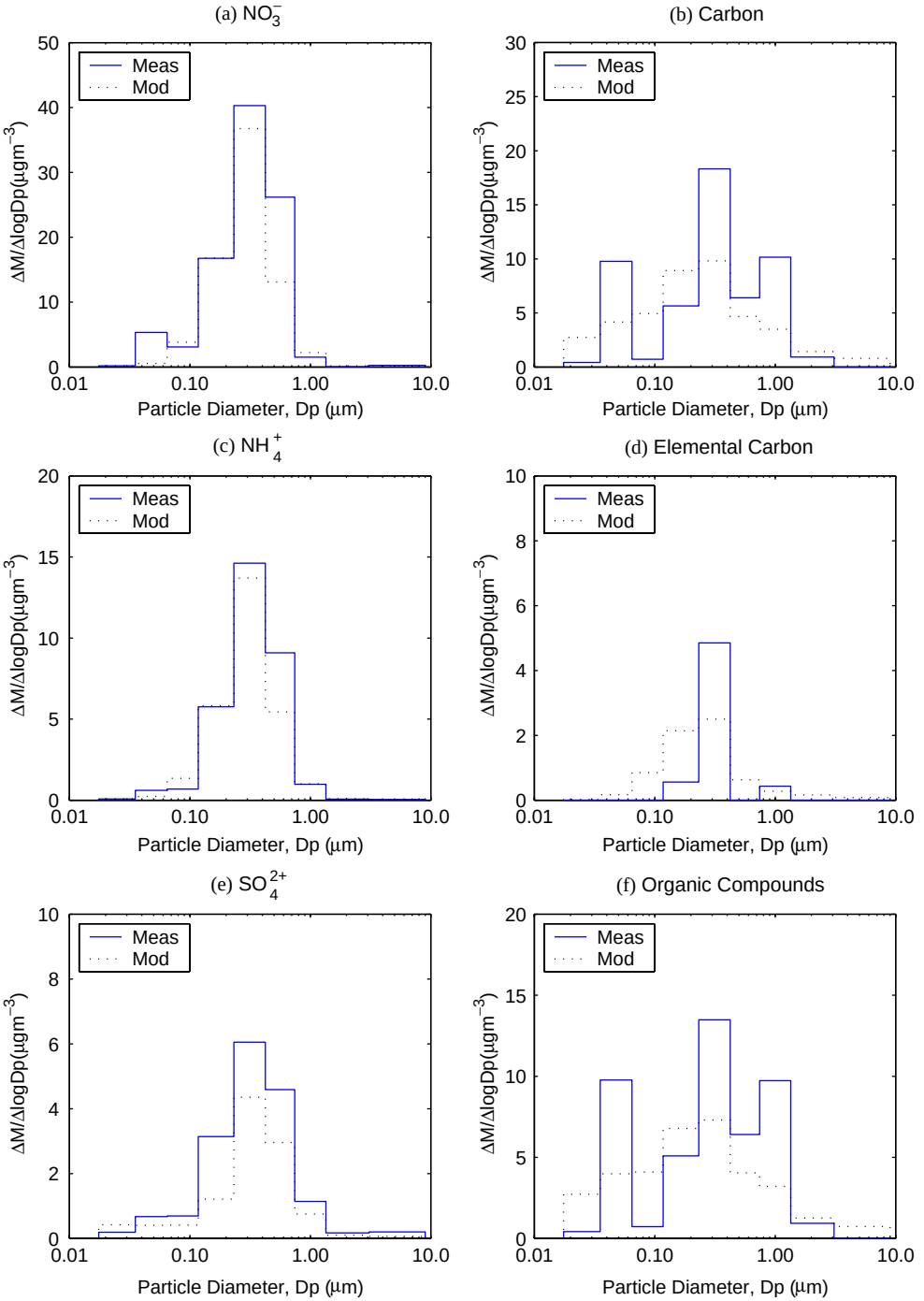

Fig. 8. Predicted (dashed line) and measured (solid line) size distributions for NO_3^-, NH_4^+, SO_4^{2-}, elemental carbon, organic compounds, and total carbon at Bakersfield between 12:00 and 15:00 on 5 January 1996. Impactor measurements have been scaled to match collocated PM_{10} filter measurements.

area under the curve for the sulfate distribution is less than its corresponding measurement area.

EC and OC, are directly emitted to the atmosphere and so their size distributions are more heavily influenced by perturbations from local sources than NO_3^-, NH_4^+, and SO_4^{2-} which are secondary pollutants and more regional in nature. The measured and modeled OC size distributions contain significant mass between

0.02 and 2.5 μm. The shape of the OC MOUDI distribution is more peaked than the near log-normal modeled distribution. Both the measured and the modeled EC size distributions peak at a diameter of 0.4 μm. Model results indicate that most of the EC mass is between 0.05 and 1.0 μm whereas measurements indicate the all EC mass is found in particles approximately 0.4 μm in diameter.

8. Conclusions

Ozone is a key indicator of atmospheric photochemical activity and strongly influences the production rates of secondary PM species such as ammonium nitrate. Based on statistical metrics and graphical time series analysis, UCD-CIT model predictions show excellent agreement with measured ozone concentrations during the IMS95 study period (excluding the Bakersfield area). The mean measured and modeled domain-averaged daily 8-h peak ozone concentrations are 26 and 22 ppb with an FBIAS of 0.16 (excluding the Bakersfield area). Within the Bakersfield area there appears to be too much fresh-NO_x in the emission inventory leading to suppressed ozone formation. Agreement with observations improves when NO_x emissions in the Bakersfield area are reduced by 25%.

Modeled regional PM_{10} and $PM_{2.5}$ concentrations show strong agreement with measurements except in the Bakersfield area where they are slightly over-predicted. PM_{10} measured mean, modeled mean, and FBIAS (with/without Bakersfield) are $(54.2/49.7)\,\mu g\,m^{-3}$, $(71.5/60.6)\,\mu g\,m^{-3}$, and $(-0.26/-0.21)$, respectively. PM_{10} mass concentrations were over predicted for short nighttime intervals at the Bakersfield core station because crustal emissions lack a realistic diurnal profile in the IMS95 emissions database. The emissions inventory near the Bakersfield area should be revised to address these issues.

Chemically speciated PM and gaseous model concentrations show good agreement with measurements. Model performance near Fresno is especially strong with carbon monoxide, ozone, NO_2, RHC, and chemically speciated PM measurements showing excellent agreement with measured concentrations. The domain-average FBIAS for ($PM_{2.5}/PM_{10}$) NO_3^-, NH_4^+, OC, EC, and SO_4^{2-} are $(-0.23/-0.17)$, $(-0.47/-0.27)$, $(-0.12/-0.02)$, $(-0.55/-0.41)$, $(-0.37/-0.20)$, respectively. The modeled size distributions for nitrate, ammonium ion, and sulfate at Bakersfield on 5 January 1996, exhibit strong agreement with measurements, and predicted OC and EC size distributions show reasonable agreement with measurements.

Overall, the CIT-UCD model is able to capture many key air quality features of the 4–6 January 1996 IMS95 air quality episode including (1) regional ozone, (2) regional PM mass, (3) chemically speciated mass at core stations, and (4) the size distribution of major PM species. Given the robust model agreement with both gas and condensed phase measurements, it appears that the CIT-UCD model adequately captures the fundamental chemistry and transport in the IMS95 domain suggesting that this model can be used to explore various control scenarios designed to improve the air quality in the SJV.

Acknowledgements

This research was supported by the San Joaquin Valleywide Air Pollution Study Agency and the California Air Resources Board under contract number 2000-05PM.

References

Alexis, A., Cox, P., Lin, A., Nguyen, C., Nystrom, M., 2002. The 2002 California Almanac of Emissions and Air Quality. California Air Resources Board, Planning and Technical Support Division.

Blanchard, C.L., Carr, E.L., Collins, J.F., Smith, T.B., Lehrman, D.E., Michaels, H.M., 1999. Spatial representativeness and scales of transport during the 1995 Integrated Monitoring Study in California's San Joaquin Valley. Atmospheric Environment 33 (29), 4775–4786.

Carter, W.P.L., 1990. A detailed mechanism for the gas-phase atmospheric reactions of organic-compounds. Atmospheric Environment Part A-General Topics 24 (3), 481–518.

Chow, J.C., Watson, J.G., Lowenthal, D.H., Solomon, P.A., Magliano, K.L., Ziman, S.D., Richards, L.W., 1992. PM10 source apportionment in California San-Joaquin Valley. Atmospheric Environment Part A-General Topics 26 (18), 3335–3354.

Chow, J.C., Watson, J.G., Lowenthal, D.H., Solomon, P.A., Magliano, K.L., Ziman, S.D., Richards, L.W., 1993. PM(10) and PM(2.5) compositions in California San Joaquin Valley. Aerosol Science and Technology 18 (2), 105–128.

Chow, J.C., Watson, J.G., Crow, D., Lowenthal, D.H., Merrifield, T., 2001. Comparison of IMPROVE and NIOSH carbon measurements. Aerosol Science and Technology 34 (1), 23–34.

Cooper, J.A., Redline, D.C., Sherman, L.N., Valdovinos, L.M., Scavone, L.C., Badgett-West, C., 1989. Final appendix V-G, PM10 source composition library for the South Coast Air Basin, technical report. South Coast Air Quality Management District, Diamond Bar, California.

Cox, W.M., Tikvart, J.A., 1990. A statistical procedure for determining the best performing air-quality simulation-model. Atmospheric Environment Part A-General Topics 24 (9), 2387–2395.

Dabdub, D., DeHaan, L.L., Seinfeld, J.H., 1999. Analysis of ozone in the San Joaquin Valley of California. Atmospheric Environment 33 (16), 2501–2514.

Eldering, A., Cass, G.R., 1996. Source-oriented model for air pollutant effects on visibility. Journal of Geophysical Research-Atmospheres 101 (D14), 19343–19369.

Goodin, W.R., McRae, G.J., Seinfeld, J.H., 1979. A comparison of interpolation methods for sparse data: application to wind and concentration fields. Journal of Applied Meteorology 18, 761–771.

Harley, R.A., Hannigan, M.P., Cass, G.R., 1992. Respeciation of organic gas emissions and the detection of excess unburned gasoline in the atmosphere. Environmental Science and Technology 26 (12), 2395–2408.

Harley, R.A., Russell, A.G., Cass, G.R., 1993. Mathematical-modeling of the concentrations of volatile organic-compounds-model performance using a lumped chemical mechanism. Environmental Science and Technology 27 (8), 1638–1649.

Hildemann, L.M., Markowski, G.R., Cass, G.R., 1991a. Chemical-composition of emissions from urban sources of fine organic aerosol. Environmental Science and Technology 25 (4), 744–759.

Hildemann, L.M., Markowski, G.R., Jones, M.C., Cass, G.R., 1991b. Submicrometer aerosol mass distributions of emissions from boilers, fireplaces, automobiles, diesel trucks and meat-cooking operations. Aerosol Science and Technology 14 (1), 138–152.

Holtzworth, G.C., 1967. Mixing depths, wind speeds, and air pollution potential for selected locations in the United States. Journal of Applied Meteorology 6, 1029–1044.

Houck, J.E., Chow, J.C., Watson, J.G., Simons, C.A., Pritchett, L.C., Goulet, J.M., Frazier, C.A., 1989. Determination of particle size distribution and chemical composition of particulate matter from selected sources in California, technical report. contract A6-175-32, California Air Resources Board; OMNI Environ. Service Incorporate; Desert Research Institute, Beaverton, Oregon.

Jacobson, M.Z., 1997. Development and application of a new air pollution modeling system 0.3. Aerosol-phase simulations. Atmospheric Environment 31 (4), 587–608.

Jacobson, M.Z., 2001. GATOR-GCMM-2. A study of daytime and nighttime ozone layers aloft, ozone in national parks, and weather during the SARMAP field campaign. Journal of Geophysical Research-Atmospheres 106 (D6), 5403–5420.

Kleeman, M.J., Cass, G.R., 2001. A 3D Eulerian source-oriented model for an externally mixed aerosol. Environmental Science and Technology 35 (24), 4834–4848.

Kleeman, M.J., Cass, G.R., Eldering, A., 1997. Modeling the airborne particle complex as a source-oriented external mixture. Journal of Geophysical Research-Atmospheres 102 (17), 21355–21372.

Kleeman, M.J., Schauer, J.J., Cass, G.R., 1999. Size and composition distribution of fine particulate matter emitted from wood burning, meat charbroiling, and cigarettes. Environmental Science and Technology 33 (20), 3516–3523.

Kleeman, M.J., Schauer, J.J., Cass, G.R., 2000. Size and composition distribution of fine particulate matter emitted from motor vehicles. Environmental Science and Technology 34 (7), 1132–1142.

Kumar, N., Lurmann, F., Pandis, S., Ansari, A., 1998. Analysis of Atmospheric Chemistry During 1995 Integrated Monitoring Study. STI-997214-1791-FR, Sonoma Technology, Inc; San Joaquin Valleywide Air Pollution Study Agency; California Air Resources Board, Sacramento, CA.

Lee, R.F., Irwin, J.S., 1995. Methodology for a comparative-evaluation of 2 air-quality models. International Journal of Environment and Pollution 5 (4–6), 723–733.

Magliano, K.L., Hughes, V.M., Chinkin, L.R., Coe, D.L., Haste, T.L., Kumar, N., Lurmann, F.W., 1999. Spatial and temporal variations in PM10 and PM2.5 source contributions and comparison to emissions during the 1995 integrated monitoring study. Atmospheric Environment 33 (29), 4757–4773.

Matthijsen, J., Slaper, H., Reinen, H., Velders, G.J.M., 2000. Reduction of solar UV by clouds: a comparison between satellite-derived cloud effects and ground-based radiation measurements. Journal of Geophysical Research-Atmospheres 105 (D4), 5069–5080.

McRae, G.J., Goodin, W.R., Seinfeld, J.H., 1982a. Development of a 2nd-generation mathematical-model for urban air-pollution 0.1. model formulation. Atmospheric Environment 16 (4), 679–696.

McRae, G.J., Goodin, W.R., Seinfeld, J.H., 1982b. Numerical-solution of the atmospheric diffusion equation for chemically reacting flows. Journal of Computational Physics 45 (1), 1–42.

Meng, Z.Y., Dabdub, D., Seinfeld, J.H., 1998. Size-resolved and chemically resolved model of atmospheric aerosol dynamics. Journal of Geophysical Research-Atmospheres 103 (D3), 3419–3435.

NIOSH, 1996. NIOSH Manual of Analytical Methods, 4th Edition. (1st Supplement). National Institute for Occupational Safety and Health, Cincinnati, OH.

Odum, J.R., Hoffmann, T., Bowman, F., Collins, D., Flagan, R.C., Seinfeld, J.H., 1996. Gas/particle partitioning and secondary organic aerosol yields. Environmental Science and Technology 30 (8), 2580–2585.

Pai, P., Vijayaraghavan, K., Seigneur, C., 2000. Particulate matter modeling in the Los Angeles basin using SAQM-AERO. Journal of the Air and Waste Management Association 50 (1), 32–42.

Pandis, S.N., Harley, R.A., Cass, G.R., Seinfeld, J.H., 1992. Secondary organic aerosol formation and transport. Atmospheric Environment Part A-General Topics 26 (13), 2269–2282.

Poli, A.A., Cirillo, M.C., 1993. On the use of the normalized mean-square error in evaluating dispersion model performance. Atmospheric Environment Part A-General Topics 27 (15), 2427–2434.

Russell, A.G., Winner, D.A., Harley, R.A., McCue, K.F., Cass, G.R., 1993. Mathematical-modeling and control of the dry deposition flux of nitrogen-containing air-pollutants. Environmental Science and Technology 27 (13), 2772–2782.

Schauer, J.J., Cass, G.R., 2000. Source apportionment of wintertime gas-phase and particle-phase air pollutants using organic compounds as tracers. Environmental Science and Technology 34 (9), 1821–1832.

Schauer, J.J., Kleeman, M.J., Cass, G.R., Simoneit, B.R.T., 1999a. Measurement of emissions from air pollution sources. 1. C-1 through C-29 organic compounds from meat charbroiling. Environmental Science and Technology 33 (10), 1566–1577.

Schauer, J.J., Kleeman, M.J., Cass, G.R., Simoneit, B.R.T., 1999b. Measurement of emissions from air pollution sources. 2. C-1 through C-30 organic compounds from medium duty diesel trucks. Environmental Science and Technology 33 (10), 1578–1587.

Schauer, J.J., Kleeman, M.J., Cass, G.R., Simoneit, B.R.T., 2001. Measurement of emissions from air pollution sources. 3. C-1–C-29 organic compounds from fireplace combustion of wood. Environmental Science and Technology 35 (9), 1716–1728.

Schauer, J.J., Kleeman, M.J., Cass, G.R., Simoneit, B.R.T., 2002a. Measurement of emissions from air pollution sources. 4. C-1–C-27 organic compounds from cooking with seed oils. Environmental Science and Technology 36 (4), 567–575.

Schauer, J.J., Kleeman, M.J., Cass, G.R., Simoneit, B.R.T., 2002b. Measurement of emissions from air pollution sources. 5. C-1–C-32 organic compounds from gasoline-powered motor vehicles. Environmental Science and Technology 36 (15), 1169–1180.

Schauer, J.J., Mader, B.T., Deminter, J.T., Heidemann, G., Bae, M.S., Seinfeld, J.H., Flagan, R.C., Cary, R.A., Smith, D., Huebert, B.J., Bertram, T., Howell, S., Kline, J.T., Quinn, P., Bates, T., Turpin, B., Lim, H.J., Yu, J.Z., Yang, H., Keywood, M.D., 2003. ACE-Asia intercomparison of a thermal-optical method for the determination of particle-phase organic and elemental carbon. Environmental Science and Technology 37 (5), 993–1001.

Seigneur, C., Pun, B., Pai, P., Louis, J.F., Solomon, P., Emery, C., Morris, R., Zahniser, M., Worsnop, D., Koutrakis, P., White, W., Tombach, I., 2000. Guidance for the performance evaluation of three-dimensional air quality modeling systems for particulate matter and visibility. Journal of the Air and Waste Management Association 50, 588–599.

Solomon, P.A., Magliano, K.L., 1999a. The 1995-Integrated Monitoring Study (IMS95) of the California Regional PM10/PM2.5 air quality study (CRPAQS): study overview. Atmospheric Environment 33 (29), 4747–4756.

Solomon, P.A., Magliano, K.L., 1999b. Objectives and design of central California's 1995 integrated monitoring study of the California regional PM10/PM2.5 air quality study. Journal of the Air and Waste Management Association 49, 199–215.

Taback, H.J., Brienza, A.R., Macko, J., Brunetz, N., 1979. Fine particle emissions from stationary and miscellaneous sources in the South Coast Air Basin, Technical Report. contract A6-191-30, California Air Resources Board; KVB Incorporated; Research-Cottrell, Tustin, California.

Ward, A.C., 1994. A simple procedure for ranking the performance of several air-quality models across a number of different sites. Atmospheric Environment 28 (18), 2909–2915.

Wexler, A.S., Seinfeld, J.H., 1991. 2nd-generation inorganic aerosol model. Atmospheric Environment Part A-General Topics 25 (12), 2731–2748.